

FINITE ELEMENT MODELING OF BEAMS WITH FUNCTIONALLY GRADED
MATERIALS

A THESIS SUBMITTED TO
THE GRADUATE SCHOOL OF NATURAL AND APPLIED SCIENCES
OF
MIDDLE EAST TECHNICAL UNIVERSITY

BY

TOLGA GÜROL

IN PARTIAL FULFILLMENT OF THE REQUIREMENTS
FOR
THE DEGREE OF MASTER OF SCIENCE
IN
CIVIL ENGINEERING

FEBRUARY 2014

Approval of the thesis:

**FINITE ELEMENT MODELING OF BEAMS WITH FUNCTIONALLY
GRADED MATERIALS**

Submitted by **TOLGA GÜROL** in partially fulfillment of the requirements of the degree of **Master of Science in Civil Engineering Department Middle East Technical University** by,

Prof. Dr. Canan Özgen
Dean, Graduate School of **Natural and Applied Sciences**

Prof. Dr. Ahmet Cevdet Yalçiner
Head of Department, **Civil Engineering**

Assoc. Prof. Dr. Afşin Sarıtaş
Supervisor, **Civil Engineering Dept., METU**

Examining Committee Members:

Assist. Prof. Dr. Serdar Göktepe
Civil Engineering Dept., METU

Assoc. Prof. Dr. Afşin Sarıtaş
Civil Engineering Dept., METU

Assoc. Prof. Dr. Yalın Arıcı
Civil Engineering Dept., METU

Assist. Prof. Dr. Ercan Gürses
Aerospace Engineering Dept., METU

Dr. Cenk Tort
MITENG

Date:

I hereby declare that all information in this document has been obtained and presented in accordance with academic rules and ethical conduct. I also declare that, as required by these rules and conduct, I have fully cited and referenced all material and results that are not original to this work.

Name, Last name: Tolga Gürol

Signature:

ABSTRACT

FINITE ELEMENT MODELING OF BEAMS WITH FUNCTIONALLY GRADED MATERIALS

Gürol, Tolga

M.Sc., Department of Civil Engineering
Supervisor: Assoc. Prof. Dr. Afşin Saritaş

February 2014, 86 PAGES

In this thesis a new beam element that is based on force formulation is proposed for modeling elastic and inelastic analysis of beams with functionally graded materials. The attempt of producing functionally graded materials (FGM) arose from mixing two materials in such a way that both of them preserve their physical, mechanical and thermal properties most effectively. FGM shows a gradation through the depth from typically a metallic material such as steel or aluminum at one face of the beam's section depth to another material such as ceramic at the other face. The change of materials properties is taken according to a power law or an exponential law.

The proposed beam element is based on the use of force interpolation functions instead of the approximation of displacement field. Since derivation of displacement interpolation functions is rather a tedious task for a beam with FGM, the proposed approach provides an easy alternative in this regard. The response of the proposed element is calculated through aggregation of responses of several monitoring sections. Section response is calculated by subdividing the depth of a monitoring section into several layers and by aggregating the material response on the layers. Since the formulation of the element is based on force interpolation functions that are

accurate under both elastic and inelastic material response, the proposed element provides robust and accurate linear and nonlinear analyses of FGM beams with respect to the displacement-based approach. For the inelastic analysis, the von Mises plasticity model with isotropic and kinematic hardening parameters is assigned for both materials for simplicity.

The consistent mass matrix for the proposed force-based element is also implemented for the validation of the vibration modes and shapes obtained from this element. For this effort, benchmark problems are both analyzed with the proposed beam element and with 3d solid elements in ANSYS. The results indicate that the proposed element provides accurate results not only in lower modes but also in higher modes of vibration.

Keywords: Functionally graded materials, finite element method, beam finite element, mixed formulation

ÖZ

FONKSİYONEL DERECELENDİRİLMİŞ MALZEMELİ KİRİŞLERİN SONLU ELEMAN MODELLEMESİ

Gürol, Tolga

Yüksek Lisans, İnşaat Mühendisliği Bölümü
Tez Yöneticisi: Doç. Dr. Afşin Sarıtaş

Şubat 2014, 86 SAYFA

Bu çalışmada, elastik ve elastik olmayan analiz modelleri için yeni bir kuvvet tabanlı fonksiyonel derecelendirilmiş malzemeli kiriş elemanı sunulmaktadır. Fonksiyonel derecelendirilmiş malzeme (FDM) üretme girişimi, her iki malzemenin fiziksel, mekanik ve termal özelliklerini en verimli şekilde koruyarak karıştırma fikrinden esinlenmiştir. Fonksiyonel derecelendirilmiş malzemeler derinlik boyunca genellikle, bir yüzdeki çelik veya alüminyum gibi metalik bir malzemedan diğer yüzdeki seramik gibi başka bir malzemeye geçiş yapar.

Sunulan kiriş elemanı yer değiştirme alanı yaklaşımı yerine kuvvet interpolasyon fonksiyonlarına dayanır. FDM'ler için yer değiştirme interpolasyon fonksiyonlarını türetmek göreceli olarak daha meşakkatli bir çalışma olduğundan, sunulan kiriş elemanı konuyla ilgili rahatlık sağlayacaktır. Sunulan kiriş elemanının tepkisi birçok kesitin tepkisinin toplanmasıyla hesaplanmıştır. Kesit tepkileri ise kirişin derinlik boyunca malzeme tepkisinin birçok katmana ayrılarak toplanmasıyla hesaplanmıştır. Eleman formülasyonu, elastik ve elastik olmayan malzeme tepkileri altında doğrulu hassas olan kuvvet interpolasyon fonksiyonlarına göre oluşturulduğu için; lineer ve lineer olmayan durumlarda, yer değiştirme tabanlı yaklaşıma göre daha doğru ve

etkin sonuçlar verir. Kolaylık açısından, her iki malzeme için de kinematik ve izotropik pekleşmeli Von Mises plastisite modeli kullanılmıştır.

Kuvvet tabanlı elemanın uyumlu kütle matrisi, titreşim modları ve şekillerinin karşılaştırması için oluşturulmuştur. Bu karşılaştırmada, ANSYS ile 3 boyutlu elemanlar kullanılarak gerçekleştirilmiştir. Sonuçlar düşük modlarda olduğu kadar yüksek modlar için de tutarlı sonuç vermektedir.

Anahtar Kelimeler: Fonksiyonel derecelendirilmiş malzeme, sonlu elemanlar yöntemi, kiriş sonlu elemanı, karma formülasyon

To My Dear Family

ACKNOWLEDGEMENTS

First of all, I want to thank to my supervisor Assoc. Prof. Dr. Afşin Sarıtaş. It would not be possible to construct this work without his motivation. He provided me all kinds of supports and help. The process would be unbearable without his priceless guidance.

Furthermore, I would like to express my sincere gratitude to Emre Özkan, Bahar İnankur, Çağatay Ata, Gürel Baltalı, Ömür Polat, Can Tezcan, Gizem Koç, Hazar Alıcı, Arda Ceyhan, Barkın Maltepli and Ceren Derici for their support and friendship.

Finally, I present my deepest gratefulness to my father Aydın Gürol, my sister İpek Gürol and my mother Filiz Gürol for their endless love and compassion.

TABLE OF CONTENTS

ABSTRACT	v
ÖZ	vii
ACKNOWLEDGEMENTS	x
TABLE OF CONTENTS	xi
LIST OF TABLES	xiii
LIST OF FIGURES	xiv
CHAPTERS	
1. INTRODUCTION.....	1
1.1. GENERAL	1
1.2. LITERATURE SURVEY	4
1.3. OBJECTIVES AND SCOPE OF THESIS	9
1.4. ORGANIZATION OF THESIS.....	10
2. FORCE-BASED ELEMENT FOR FGM BEAMS.....	13
2.1. FORCE-DEFORMATION RELATIONS OF FRAME ELEMENT WITH SHEAR DEFORMATIONS (TIMOSHENKO BEAM THEORY)	13
2.2. SECTION KINEMATICS	15
2.2.1. Euler-Bernoulli Beam Theory.....	16
2.2.2. Timoshenko’s Beam Theory	17
2.3. TRANSFORMATION BETWEEN BASIC SYSTEM AND COMPLETE SYSTEM.....	21
2.4. STATE DETERMINATION OF FORCE-BASED ELEMENT	23
2.5. THE CONVERGENCE RATE OF NEWTON–RAPHSON METHOD...	27
2.6. FORCE-BASED CONSISTENT MASS MATRIX	29
3. A DISPLACEMENT-BASED ELEMENT FOR FGM BEAMS	33
3.1. FORMULATION OF DISPLACEMENT-BASED ELEMENT	33
3.2. THE CONSISTENT MASS MATRIX.....	40
4. MODELING INELASTIC BEHAVIOR OF FGM BEAMS	43
4.1. VON MISES PLASTICITY	43

4.2. VON MISES PLASTICITY WITH LINEAR ISOTROPIC AND KINEMATIC HARDENING.....	45
4.3. STRESS UPDATE ALGORITHM FOR HARDENING PLASTICITY ..	48
5. VERIFICATION OF THE PROPOSED BEAM ELEMENT	53
5.1. COMPARISON OF INELASTIC BEHAVIORS	53
5.2. COMPARISON OF VIBRATION CHARACTERISTICS	64
6. CONCLUSIONS.....	81
6.1. SUMMARY	81
6.2. CONCLUSIONS.....	81
6.3. RECOMMENDATIONS FOR FUTURE STUDY.....	82
REFERENCES.....	83
APPENDICES.....	85
A. DEFINITION OF VARIATION	85

LIST OF TABLES

TABLES

Table 1 Strong and Weak Satisfaction of Parameters in Variational Principles.....	8
Table 2 $L/d = 5$ Comparison of element responses for varying discretizations.....	59
Table 3 Computation times of several analyses with different element numbers and formulation types ($nIP = 5$, number of layers = 21).....	62
Table 4 Material properties at each layer of the ANSYS model.....	66
Table 5 $L/d = 10$ Vibration frequencies and shapes for homogenous section made of steel	67
Table 6 $L/d = 5$ Vibration frequencies and shapes for homogenous section made of steel	68
Table 7 $L/d = 2$ Vibration frequencies and shapes for homogenous section made of steel	70
Table 8 $L/d = 10$ Vibration frequencies and shapes for 4 layers of FGM section.....	72
Table 9 $L/d = 5$ Vibration frequencies and shapes for 4 layers of FGM section.....	73
Table 10 $L/d = 2$ Vibration frequencies and shapes for 4 layers of FGM section.....	75
Table 11 Frequency comparison of proposed beam element and ANSYS model for rectangular steel section $d=100$ mm and $b=100$ mm	77
Table 12 Frequency comparison of proposed beam element and ANSYS model for FGM section $d=100$ mm and $b=100$ mm.....	78

LIST OF FIGURES

FIGURES

Figure 1 Organic and artificial illustrations for FGM Jha et al. (2013)	2
Figure 2 Variation of material properties on the depth of FGM beams	7
Figure 3 Simply supported basic system for force-based beam element	13
Figure 4 Nodal end forces and beam statics for force-based beam	14
Figure 5 Arbitrary cross-section for a solid beam element	16
Figure 6 Various FGM sections for different values of n	19
Figure 7 Distribution of ingredients for different values of n	20
Figure 8 Conversion from simply supported system to 2 node beam element	22
Figure 9 Visualization of Newton–Raphson iterations	28
Figure 10 Coordinate system for the finite element model	33
Figure 11 Visualization of the von Mises yield surface	45
Figure 12 Visualization of the von Mises plasticity with isotropic and kinematic hardening through the principal stress state	51
Figure 13 Inelastic Loading Example	54
Figure 14 One force-based element per half-span and $nIP = 3$	56
Figure 15 One force-based element per half-span and $nIP = 5$	56
Figure 16 One force-based element per half-span and $nIP = 10$	57
Figure 17 One displacement-based element per half-span and $nIP = 3$	57
Figure 18 One displacement-based element per half-span and $nIP = 5$	58
Figure 19 One displacement-based element per half-span and $nIP = 10$	58
Figure 20 Four force-based elements per half-span and $nIP = 5$	59
Figure 21 Load-Deflection curve for several numbers of elements (DB and FB)	60
Figure 22 Bending moment distribution along the length of beam	61
Figure 23 Curvature distribution along the length of beam	61
Figure 24 Axial force distribution along the length of beam	62
Figure 25 Normal stress distribution	63
Figure 26 Shear stress distribution	64

Figure 27 Visualization of ANSYS FGM beam model 65

CHAPTER 1

INTRODUCTION

1.1. GENERAL

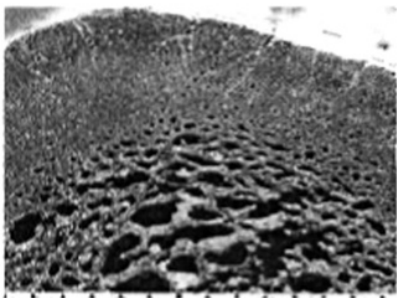
Materials have played a significant role in society throughout the history. Mankind always tried to produce stronger materials for building durable structures for shelter. In early ages of civilization (1500 BC) Egyptians and Mesopotamians mixed straw and mud to form bricks for constructing tougher and more enduring buildings. Afterwards in 1800 AD, concrete became a widely used composite, which is created by mixing cement, aggregate and water. Later, in early 1900's, fiber reinforced plastics, a composite consisting of a polymer matrix reinforced with fibers, ended up as an essential material for aerospace, automotive, marine and construction industries.

A preferable way of combining two materials, preserving their properties, is to combine them by a varying percentage over the cross section. For example, attaching a ceramic surface at the top and a steel surface at the bottom with a smooth transition zone, so called the functionally graded materials (FGM), is accepted as a better way of bonding rather than sticking them directly without gradation.

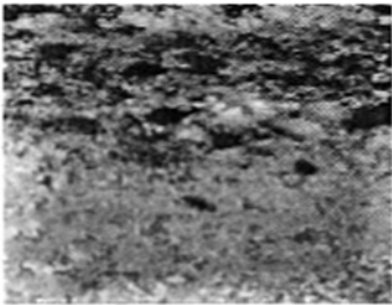
By this procedure, both materials protect their best properties – like high strength, high stiffness, high temperature resistance and low density of ceramics and toughness and malleability of steel.

FGMs are being used in several industries and sectors like aerospace, nuclear, defense, automotive, communication, energy etc. As well as they are produced artificially, the primitive forms of FGMs exist in nature. Bones, human skin, bamboo

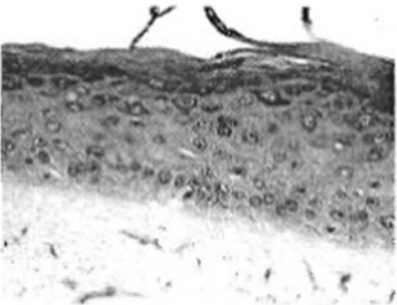
tree can be considered as organic forms of FGM. Figure 1 illustrates several organic and artificial examples that evoke FGM.



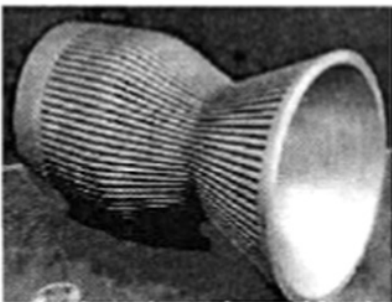
Bone^a



Thermal coating^d



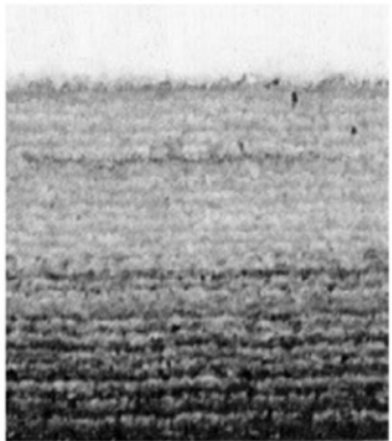
Human skin^b



Rocket casing^e



Bamboo Tree^c



Ceramic-metal FGM^f

Figure 1 Organic and artificial illustrations for FGM Jha et al. (2013)

The application areas of FGMs can be summarized as follows:

Aerospace: Spacecraft heat shields, heat exchanger tubes

Biomedical: Artificial bones, skins, teeth

Communication: Optical fibers, lenses, semiconductors

Nuclear field: Fuel palettes, plasma wall of fusion reactors

Energy sector: Thermoelectric generators, solar cells, sensors

Automotive: Power transmission systems, braking systems.

The theoretical concept of producing FGM was proposed in 1984 in Japan (Jha et al. (2013)). Manufacturing and design process of FGM has become the main topic of interest in the last three decades. Manufacturing of FGMs can be discussed under two subtopics which are gradation and consolidation. Gradation is forming the spatially inhomogeneous structure. Gradation processes can be categorized into constitutive, homogenizing and segregating processes. Constitutive processes depend on a stepwise generation of the graded body from pioneer materials or powders. Advances in automation technology in course of the last decades have provided technological and economic viability for constitutive processes. Homogenization is conversion of the sudden transition between two materials into a gradient. Segregating processes start with a macroscopically homogenous material which is transformed into a graded material by material transport caused by an external field (for example gravitational or magnetic field). Homogenizing and segregation processes yield continuous gradients; but such processes have limitations concerning the distribution of materials to be produced.

The consolidation processes, such as drying, sintering or solidification, usually comes after the gradation processes. The processing criterions should be determined in such a way that the gradient is not wrecked or changed in an unrestrained fashion (Kieback et al. (2003)).

1.2. LITERATURE SURVEY

With the aim of moving onto the more effective production and use of FGM materials in engineering applications, several analysis techniques have been proposed, as well. Most of the analyses of structural members with FGM are based on theory of elasticity solution techniques in literature. It is worth mentioning that such analyses offer load and boundary condition specific solutions to the problem and also focus on linear elastic behaviors of materials only.

An alternative to such analysis would be the development of plate, shell or solid finite elements that will enable analysis of problems with FGM. It is worth mentioning that even the available packages like ANSYS or ABAQUS do not automatically provide such capabilities and require the development of user-defined subroutines and functions.

As can be indicated from Figure 1 and examples concerning the usage areas of FGM mentioned above (thermal coating, heat shields, rocket casing etc.), shell and plate elements are a way more preferable for modeling tools for such structures. For this purpose, a study has been performed by Reddy and Chin (1998) for the mechanical and thermal behavior of shell elements with FGM. A finite shell element for the analysis of FGM is developed in that study and parametric studies of the thermo-mechanical coupling effect on FGM are also carried out. The parameters are selected as the distribution ratios of the materials and types of materials. The outcomes of the coupled formulation and uncoupled formulation are compared with each other. For the example with ceramic-rich top surface and metal-rich bottom surface plate element with FGM, the following statements are concluded in that study. The temperature fields for coupled and uncoupled formulations show little difference but this difference diminishes as time goes on. On the contrary, the difference between the displacement fields, for the coupled and uncoupled formulations, starts to increase as time progresses; but this difference decreases as the ratio of ceramic material increases.

In the study of Reddy (2000), the thermo-mechanical behaviors of plates with FGM have been analyzed using finite element formulation making use of von Karman type large strain formulation. Nonlinear first-order plate theory and linear third-order plate theory have been used for the analyses. The results indicate that, the basic response of the plates with FGM that are constituted by metal and ceramics, do not necessarily lie between the full metal and full ceramic states. The non-dimensional deflection was found to reach a minimum at a volume fraction index that depends on the properties and the ratio of the properties of the constituents.

An alternative finite element modeling approach compared to shell or plate element is the development of beam finite elements. Beam theories describe section kinematics of a beam element, and the beam theories are grouped under Euler-Bernoulli, Timoshenko and Higher Order beam theories in the literature. Development of beam finite elements through the use of various beam theories is mainly categorized in two, where the most widely adopted choice is the use of displacement-based approach and the alternative method is the use of mixed formulation approach. Within the context of displacement-based formulations and Timoshenko beam theory assumptions for uniform prismatic beams with homogeneous materials, beam finite elements proposed by Friedman and Kosmatka (1993) and Reddy (1997) prove to be a shear-locking free element and provide the exact the stiffness matrix under linear elastic response.

In terms of development of beams with FGM, the earliest and the most popularly cited work is the beam finite element proposed by Chakraborty et al. (2003) in which they developed a new beam element to study the thermo-elastic reactions of FGM beams. The generation of shape functions, stiffness and mass matrix for FGM beam has been explained in that research. The stiffness matrix is free of shear locking since the degree of transverse displacement shape function is higher than the slope shape function as discussed by Reddy (1997). Numerical examples concerning the thermal and static loadings, free vibration and wave propagation results are also attached to the research. It is worth mentioning that the study by Chakraborty et al. (2003) is

popularly cited in the literature and is considered as a benchmark formulation for FGM beams.

Stability analysis of functionally graded beams has been carried out in the study by Mohanty et al. (2011) through the use of the finite element proposed by Chakraborty et al. (2003). In that work, the researchers examined the dynamic stability of functionally graded ordinary beams and functionally graded sandwich beams on Winkler's elastic foundation. Functionally graded ordinary (FGO) beams consist of first material 100% at top of the section; second material 100% at the bottom of the section with a transition zone from topmost to bottommost of the section. Whereas, in functionally graded sandwich (FGSW) beams; the transition zone appears as a core material between first material at the top with a finite thickness and second material at the bottom likewise. In Figure 2 section (A) represents the functionally graded sandwich beam and section (B) represents the functionally graded ordinary beam in which the transition is through the whole section. In that work, it is concluded that for a functionally graded sandwich beam; if the materials vary with respect to the power law the beam becomes less stable as the thickness of the FGM core increases. In the other case, as the materials vary according to exponential law, an increase in the thickness of the FGM core improves the stability of the beam.

In study by Hemmatnezhad et al. (2013), large amplitude free vibration analysis, imposing von Karman type of large strain, of beams with functionally graded materials, is realized. The finite beam element formulation for FGM, proposed by Chakraborty et al. (2003) has been used in that study, as well. The results obtained from numerical simulations are compared with theory of elasticity solutions available in the literature.

Besides the development and use of displacement-based finite elements, it is also possible to formulate mixed formulation finite elements for the analysis of FGM beams. In the literature, it appears that there is no such element proposed and used for the analysis of beams with FGM. It is furthermore worth to mention that inelastic analysis of FGM members has not been undertaken in the context of beam finite

elements. In a study by Bocciarelli et al. (2008) the use of Von Mises plasticity model for metallic materials and Drucker-Prager plasticity model for ceramic type materials have been proposed for the analysis of FGM members. In that study, solid finite elements have been used for modeling FGM. Identification of the material parameters of FGM requires both experimental studies and analytical validation, and this requires significant amount of effort. In this thesis, an effort is also demonstrated for the inelastic analysis of FGM beams.

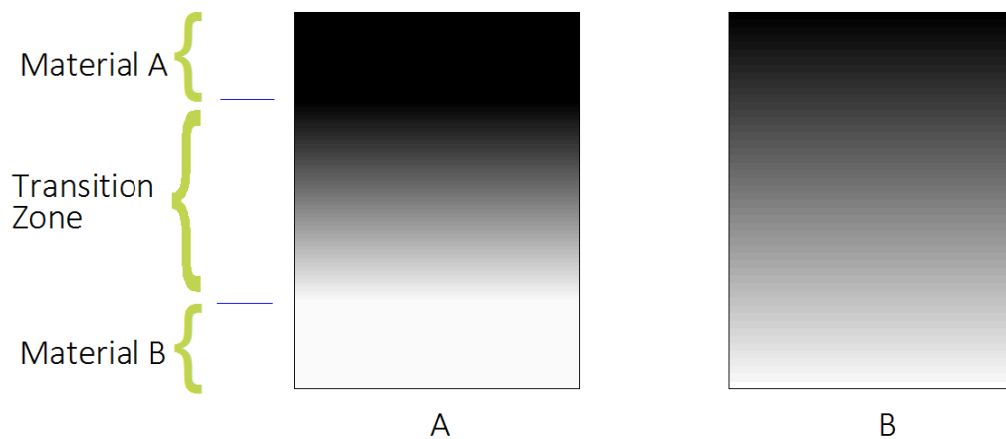


Figure 2 Variation of material properties on the depth of FGM beams

For the sake of completeness of literature survey, the development and use of force-based and mixed formulation beam finite elements is also presented in this part. Since the proposed beam element actually bases on the same assumptions of the initial force-based element proposed in the literature, such a presentation is necessary in order to point out also the differences of the element proposed in this thesis. Displacement-based elements are formulated within the context of principle of virtual displacements or more generally called as principle of minimum potential energy. In this approach, displacement fields are the independent variables. In mixed formulation approaches, stress and strain fields are also brought into the functional and the satisfaction of the equations are weakened. A summary of the strong and weak satisfaction of variational principles are listed in Table 1. For the description of the fields listed in the table, refer to the work by Saritas and Soydas (2012).

Table 1 Strong and Weak Satisfaction of Parameters in Variational Principles

Varied Fields	Functional Name	Strong Satisfaction	Weak Satisfaction
\mathbf{u}	Potential Energy	$\boldsymbol{\varepsilon} = \nabla^s \mathbf{u}$ on Ω $\boldsymbol{\sigma} = \boldsymbol{\sigma}(\boldsymbol{\varepsilon})$ on Ω $\mathbf{u} = \mathbf{u}^*$ on Γ_u	$\text{div } \boldsymbol{\sigma} + \mathbf{b} = \mathbf{0}$ on Ω $\mathbf{t} = \mathbf{t}^*$ on Γ_t
$\boldsymbol{\sigma}$	Complementary Energy	$\text{div } \boldsymbol{\sigma} + \mathbf{b} = \mathbf{0}$ on Ω $\boldsymbol{\sigma} = \boldsymbol{\sigma}(\boldsymbol{\varepsilon})$ on Ω $\mathbf{t} = \mathbf{t}^*$ on Γ_t	$\boldsymbol{\varepsilon} = \nabla^s \mathbf{u}$ on Ω $\mathbf{u} = \mathbf{u}^*$ on Γ_u
$\mathbf{u}, \boldsymbol{\sigma}$	Hellinger-Reissner	$\boldsymbol{\varepsilon} = \nabla^s \mathbf{u}$ on Ω $\mathbf{u} = \mathbf{u}^*$ on Γ_u	$\text{div } \boldsymbol{\sigma} + \mathbf{b} = \mathbf{0}$ on Ω $\boldsymbol{\sigma} = \boldsymbol{\sigma}(\boldsymbol{\varepsilon})$ on Ω $\mathbf{t} = \mathbf{t}^*$ on Γ_t
$\boldsymbol{\sigma}, \boldsymbol{\varepsilon}$	No name	$\text{div } \boldsymbol{\sigma} + \mathbf{b} = \mathbf{0}$ on Ω $\mathbf{t} = \mathbf{t}^*$ on Γ_t	$\boldsymbol{\varepsilon} = \nabla^s \mathbf{u}$ on Ω $\boldsymbol{\sigma} = \boldsymbol{\sigma}(\boldsymbol{\varepsilon})$ on Ω $\mathbf{u} = \mathbf{u}^*$ on Γ_u
$\mathbf{u}, \boldsymbol{\sigma}, \boldsymbol{\varepsilon}$	Hu-Washizu	-	$\text{div } \boldsymbol{\sigma} + \mathbf{b} = \mathbf{0}$ on Ω $\boldsymbol{\varepsilon} = \nabla^s \mathbf{u}$ on Ω $\boldsymbol{\sigma} = \boldsymbol{\sigma}(\boldsymbol{\varepsilon})$ on Ω $\mathbf{u} = \mathbf{u}^*$ on Γ_u $\mathbf{t} = \mathbf{t}^*$ on Γ_t

The last two decades witnessed the development and further improvement of the nonlinear force-based beam element proposed by Spacone et al. (1996). In this regards, detailed literature survey is provided by Saritas (2006) and Soydas (2013). Variational base of force-based beam elements is recently shown by Saritas and Soydas (2012) to be the same as that of mixed formulation approach, and it was shown that the use of Hellinger-Reissner or Hu-Washizu functionals provide the mathematical base of the force-based elements.

Initial and the most widely cited work in terms of development of a nonlinear force-based beam finite element was first documented in detail by Spacone et al. (1996). The element sets forward to the consistent numerical implementation of the element state determination in the context of a standard FEM package. For the displacement-based finite elements the iterative process depends on the residual forces whereas for the proposed element, the procedure is based on the residual deformations.

In a recent study by Soydas and Saritas (2013), an accurate nonlinear 3d beam finite element is proposed for inelastic analysis of solid and hollow circular sections. The element is based on Hu-Washizu functional and axial force, shear forces, bending moments about both axes and torsional moment is coupled through the use of 3d material models and fiber discretization of the section and the use of several monitoring sections along element length. The element proposed in that work proved to be very effective in capturing the behavior of long and short members that are loaded and restrained in various fashions.

1.3. OBJECTIVES AND SCOPE OF THESIS

In this thesis, the development of a force-based beam element for the analysis of functionally graded materials is considered. The beam element that is developed in this thesis is based on the use of force interpolation functions instead of the approximation of displacement field. The response of the proposed element is calculated through aggregation of responses of several monitoring sections. Section response is calculated by subdividing the depth of a monitoring section into several layers and by aggregating the material response on the layers. Since the formulation of the element bases on force interpolation functions that are accurate under both elastic and inelastic material response, the proposed element provides robust and accurate linear and nonlinear analysis of FGM beams with respect to displacement-based approach. The formulated element is compared with a previously developed displacement-based beam finite element by Chakraborty et al. (2003).

For inelastic analysis, von Mises plasticity model with isotropic and kinematic hardening parameters is assigned for both materials for simplicity. A simply supported pin-pin FGM beam is divided into different numbers of elements (both force-based and displacement-based beam elements), and the simply supported system is exposed to support vertical displacement from the mid-span. The results indicate the accuracy and robustness of the proposed element over the displacement-based element in terms of global level response as well as local measures such as forces and stresses.

The second effort in this thesis focuses on the vibration characteristics of the proposed beam element with FGM. Consistent mass matrix for the force-based element is implemented for the validation of the vibration modes and shapes obtained from this element. For this effort, benchmark problems are both analyzed with proposed beam element and with 3d solid elements in ANSYS. The results indicate that proposed element provides not only accurate results in lower modes but also in higher modes of vibration.

1.4. ORGANIZATION OF THESIS

In the second chapter force-deformation relations of proposed beam element will be presented and some principal beam theories and their section kinematics will be mentioned. Then, the implementation of force-based elements into a nonlinear FEM package and the convergence rate of the Newton–Raphson iteration procedure will be discussed and derivation of the stiffness matrix and the consistent mass matrix for the proposed force-based beam element will be presented.

In the third chapter; a previously developed displacement-based beam element for FGM will be provided for the sake of completeness of the thesis work. The formulations for the element will be discussed in detail, where it was observed that some of the coefficients presented in the original work required correction.

In the fourth chapter; the material model, which is selected to mimic the behavior of materials in the FGM section, has been formulated. The radial return mapping algorithm for the von Mises plasticity has been presented.

In the fifth chapter numerical analyses for the proposed beam element will be held out. Firstly, non-linear analysis will be realized for the force-based element and then the results will be compared with the displacement-based element. Secondly, modal analyses will be realized for the proposed force-based finite beam element. The modal shapes and natural frequencies will be compared with the results obtained from ANSYS.

Finally in the sixth chapter, conclusion and recommendations for further studies will be documented.

CHAPTER 2

FORCE-BASED ELEMENT FOR FGM BEAMS

In this chapter, first, force-deformation relations of frame element will be clarified, and then some principal beam theories and their section kinematics will be mentioned. Thirdly, the implementation of force-based elements into a nonlinear FEM package and the convergence rate of the Newton–Raphson iteration procedure will be discussed. Development of the proposed beam element is done in a basic system where rigid body modes are eliminated. For this reason, conversion of the beam response from the basic system to the complete system is cast in this chapter after the formulation of the beam element in the basic system. Finally, derivation of the consistent mass matrix for the force-based beam element is explained.

2.1. FORCE-DEFORMATION RELATIONS OF FRAME ELEMENT WITH SHEAR DEFORMATIONS (TIMOSHENKO BEAM THEORY)

In this subtopic the element force relations, force shape functions and the derivation of section flexibility and stiffness matrices will be clarified.



Figure 3 Simply supported basic system for force-based beam element

Figure 3 shows the element end forces of a simply supported (pin-pin) basic system. In the absence of element loads the axial force and shear force distribution is constant and moment distribution is linear with respect to x-axis.

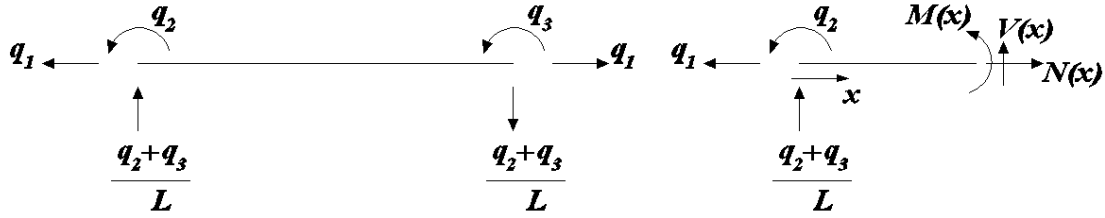


Figure 4 Nodal end forces and beam statics for force-based beam

From Figure 4 the axial force, shear force and moment equations can be derived through simple statics knowledge as follows

$$\begin{aligned}
 N(x) &= q_1 \\
 M(x) &= \left(\frac{x}{L} - 1\right)q_2 + \left(\frac{x}{L}\right)q_3 \\
 V(x) &= -(q_2 + q_3)/L
 \end{aligned} \tag{2.1}$$

Equation (2.1) can be written in matrix notation as

$$\underline{s}(x) = \begin{Bmatrix} N(x) \\ M(x) \\ V(x) \end{Bmatrix} = \begin{bmatrix} 1 & 0 & 0 \\ 0 & x/L - 1 & x/L \\ 0 & -1/L & -1/L \end{bmatrix} \begin{Bmatrix} q_1 \\ q_2 \\ q_3 \end{Bmatrix} = \underline{b}(x)\underline{q} \tag{2.2}$$

In (2.2), the section forces, force interpolation (equilibrium) matrix and element force vector will be shown as $\underline{s}(x)$, $\underline{b}(x)$ and \underline{q} , respectively.

Now if the principle of virtual forces is used, the following equality can be written.

$$\delta \underline{q}^T \underline{v} = \int_0^L \delta \underline{s}^T(x) \underline{e}(x) dx \tag{2.3}$$

In (2.3), $\underline{e}(x)$ represent the section deformations, where the components of this vector will be mentioned later in this chapter.

The same interpolation functions have been selected for the force field and the virtual force field, thus

$$\delta \underline{s}^T(x) = \delta \underline{q}^T \underline{b}^T(x) \quad (2.4)$$

Inserting (2.4) into (2.3) we obtain the element deformation vector \underline{v} in the basic system as follows

$$\underline{v} = \int_0^L \underline{b}^T(x) \underline{e}(x) dx \quad (2.5)$$

Making use of the chain rule, flexibility matrix of the beam element is obtained.

$$\underline{f} = \frac{\partial \underline{v}}{\partial \underline{q}} = \int_0^L \underline{b}^T(x) \underbrace{f_s}_{\frac{\partial \underline{e}(x)}{\partial \underline{s}(x)}} \underbrace{\underline{b}(x)}_{\frac{\partial \underline{s}(x)}{\partial \underline{q}}} dx \quad (2.6)$$

In (2.6) \underline{f} is the element flexibility matrix. The terms $\frac{\partial \underline{e}(x)}{\partial \underline{s}(x)}$ and $\frac{\partial \underline{s}(x)}{\partial \underline{q}}$ are written as \underline{f}_s and $\underline{b}(x)$, respectively. The matrix \underline{f}_s , so called section flexibility matrix can be computed from the inverse of the section stiffness matrix through the relation $\underline{f}_s = \underline{k}_s^{-1}$. Section stiffness matrix \underline{k}_s will be introduced in the next subtopic.

2.2. SECTION KINEMATICS

In this part two beam theories and their section characteristics will be mentioned. First the Euler-Bernoulli beam theory will be represented, where the plane sections remain plane and the angle between the normal of the section and tangent to the deformed axis of the beam is zero, thus no shear deformation takes place in this

beam theory. The second one is, Timoshenko's beam theory, where in this theory plane sections remain plane likewise, but the angle between the normal of section and the tangent to the deformed axis of the beam is not necessarily equal to zero. According to Timoshenko's beam theory the beam element can exhibit shear deformations.

There are also other beam theories where the plane sections do not have to remain plane, so called higher order beam theories. A discussion of higher order beam theories is available in the paper by Reddy (1997).

2.2.1. Euler-Bernoulli Beam Theory

Figure 5 shows the cross section of a beam element. An arbitrary point P is described on the cross section.

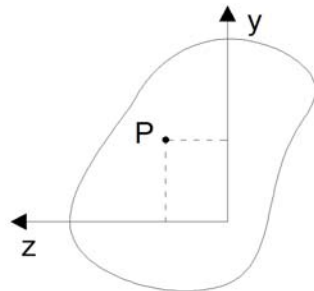


Figure 5 Arbitrary cross-section for a solid beam element

Assuming that Euler-Bernoulli beam theory assumptions hold, we can only calculate a non-zero strain value that is the normal strain, and it is expressed as follows

$$\varepsilon(x, y, z) = \varepsilon_a(x) - y\kappa_z(x) + z\kappa_y(x) \quad (2.7)$$

Since our analysis is in 2d, we do not seek for moments around y axis; thus curvature about y axis is not taken into account, and Equation (2.7) can be simplified as

$$\varepsilon_x = \varepsilon_a(x) - y\kappa(x) \quad (2.8)$$

Hereupon, the curvature about z axis is simply denoted with κ . We can show (2.8) in vector notation as

$$\boldsymbol{\varepsilon}_x = [1 \quad -y] \begin{Bmatrix} \boldsymbol{\varepsilon}_a(x) \\ \kappa(x) \end{Bmatrix} \quad (2.9)$$

2.2.2. Timoshenko's Beam Theory

The difference between Timoshenko and Euler – Bernoulli beam theories is that, the plane sections after deformation will not remain normal to deformed axis of the beam; thus another deformation variable on the section γ is introduced to represent the angle difference between the normal to the section and the tangent to the deformed axis of the beam.

Rest of the formulations in this chapter will constitute utilization of the Timoshenko beam theory section kinematics, where the strains on the section of a 2d beam element can be written as follows

$$\begin{Bmatrix} \boldsymbol{\varepsilon}_x \\ \gamma_{xy} \end{Bmatrix} = \begin{bmatrix} 1 & -y & 0 \\ 0 & 0 & 1 \end{bmatrix} \begin{Bmatrix} \boldsymbol{\varepsilon}_a \\ \kappa \\ \gamma \end{Bmatrix} \quad (2.10)$$

or

$$\begin{Bmatrix} \boldsymbol{\varepsilon}_x \\ \gamma_{xy} \end{Bmatrix} = \underline{a}_s \underline{e}(x) \quad (2.11)$$

where γ is the shear deformation of section on the x-y plane in (2.10), \underline{a}_s is the 2x3 compatibility matrix and \underline{e} is the 3x1 section deformation vector in (2.11).

Now we will establish the relation between section forces and section deformations.

$$\underline{s}(x) = \int_A \underline{a}_s^T \underline{\sigma} dA \quad (2.12)$$

where

$$\underline{\sigma} = \begin{Bmatrix} \sigma_x \\ \tau_{xy} \end{Bmatrix} = \begin{bmatrix} E & 0 \\ 0 & G \end{bmatrix} \begin{Bmatrix} \epsilon_x \\ \gamma_{xy} \end{Bmatrix} \quad (2.13)$$

$$\underline{s}(x) = \begin{Bmatrix} N(x) \\ M(x) \\ V(x) \end{Bmatrix} \quad (2.14)$$

$\underline{s}(x)$ is the vector of section forces, where N , M and V are axial force through x axis, moment about z axis and shear force along y axis, respectively.

Substituting (2.11) and (2.13) into (2.12) we get

$$\underline{s}(x) = \left[\int_A \underline{a}_s^T \begin{bmatrix} E & 0 \\ 0 & G \end{bmatrix} \underline{a}_s dA \right] \underline{\epsilon}(x) \quad (2.15)$$

Where the term in brackets is \underline{k}_s which is called the section stiffness matrix. If the material properties do not vary through the section depth, section stiffness matrix can be written as follows

$$\underline{k}_s = \int_A \begin{bmatrix} E & -yE & 0 \\ -yE & y^2E & 0 \\ 0 & 0 & G \end{bmatrix} dA = \begin{bmatrix} EA & -EQ & 0 \\ -EQ & EI & 0 \\ 0 & 0 & GA \end{bmatrix} \quad (2.16)$$

Where, I is the moment of inertia about the bending axis, Q is the first moment of the area about the bending axis, and if the bending axis matches with the geometric centroid then Q is equal to zero. In above equation, GA term is usually corrected for the presence of non-uniform distribution of shear over the section, and $\kappa_s GA$ is substituted instead of GA .

Since we are dealing with FGM; Young modulus (E) and shear modulus (G) vary through the depth of the section. So, the modulus matrix cannot be taken outside the integral. For FGM sections \underline{k}_s must be computed as follows

$$k_s = \int_A a_s^T \begin{bmatrix} E(y) & 0 \\ 0 & G(y) \end{bmatrix} a_s dA \quad (2.17)$$

Generally two types of material distribution functions are used for FGM. These are the exponential law and power law. The exponential law is frequently used in fracture studies for FGM, but it does not display curvature for both directions.

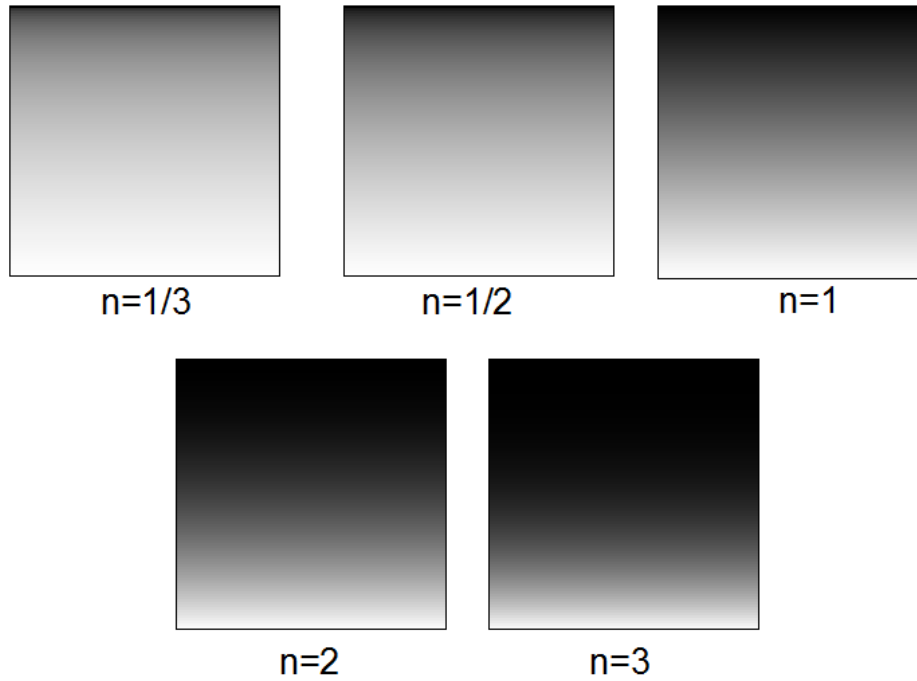


Figure 6 Various FGM sections for different values of n

The exponential law can be indicated as follows Chakraborty et al. (2003).

$$\begin{aligned} \varphi(y) &= \varphi_t \exp\left(-\delta\left(1 - \frac{2y}{h}\right)\right) \\ \delta &= \frac{1}{2} \log\left(\frac{\varphi_t}{\varphi_b}\right) \end{aligned} \quad (2.18)$$

Likewise, the power law can be written as

$$\varphi(y) = (\varphi_t - \varphi_b) \left(\frac{y}{h} + \frac{1}{2} \right)^n + \varphi_b \quad (2.19)$$

Here $\varphi(y)$ represents the material properties such as elastic modulus, shear modulus, thermal expansion coefficient, mass density etc. φ_t and φ_b stand for the topmost and bottommost materials, respectively. It is suggested that the power coefficient n can be taken between 1/3 and 3. Otherwise, FGM would contain too much of one phase (1/3 or 3 contributes to %75 of total volume) (refer to the work by Nakamura et al. (2000)).

Figure 6 and Figure 7 show the material distribution for several FGM sections with different power law coefficients (n).

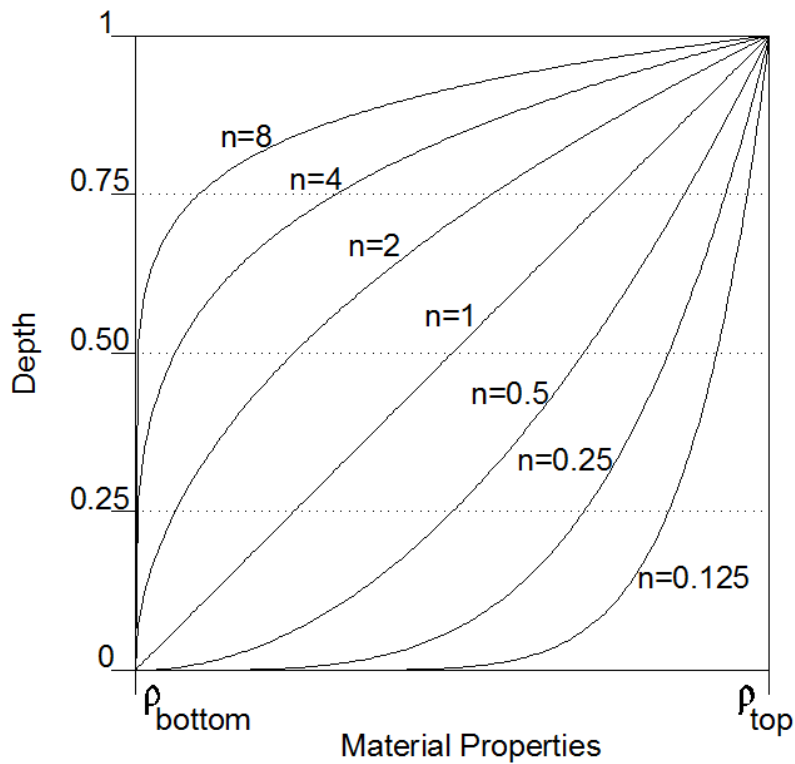


Figure 7 Distribution of ingredients for different values of n

2.3. TRANSFORMATION BETWEEN BASIC SYSTEM AND COMPLETE SYSTEM

In this part, conversion from simply supported (pin-pin) basic system to the complete system will be discussed. In the basic system, rigid body modes of displacements are eliminated, thus there are only the element deformations.

In 2d case, there are three element deformations, namely the axial deformation and the two end rotations for the simply supported basic system. We can also choose cantilever basic system as an alternative, and in that case assuming the left end fixed, there will be one axial deformation, one transverse displacement and one rotation as element deformations existing on the right end of the element.

In the complete system, the element has two nodes and at each node there are 3 degrees of freedom, i.e. the translations along and transverse to the element and the rotation at that node.

The necessity of the transformation between the basic system and the complete system stems from the formulation of the force-based element in the basic system and the fact that the FEM program will provide nodal displacements in the complete system.

From Figure 8, making use of the small deformation theory, the compatibility equations between element deformations and nodal displacements are derived as follows:

$$\begin{aligned}v_1 &= u_4 - u_1 \\v_2 &= u_3 - \alpha \\v_3 &= u_6 - \alpha\end{aligned}\tag{2.20}$$

$$\text{where } \alpha = \frac{(u_5 - u_2)}{L}$$

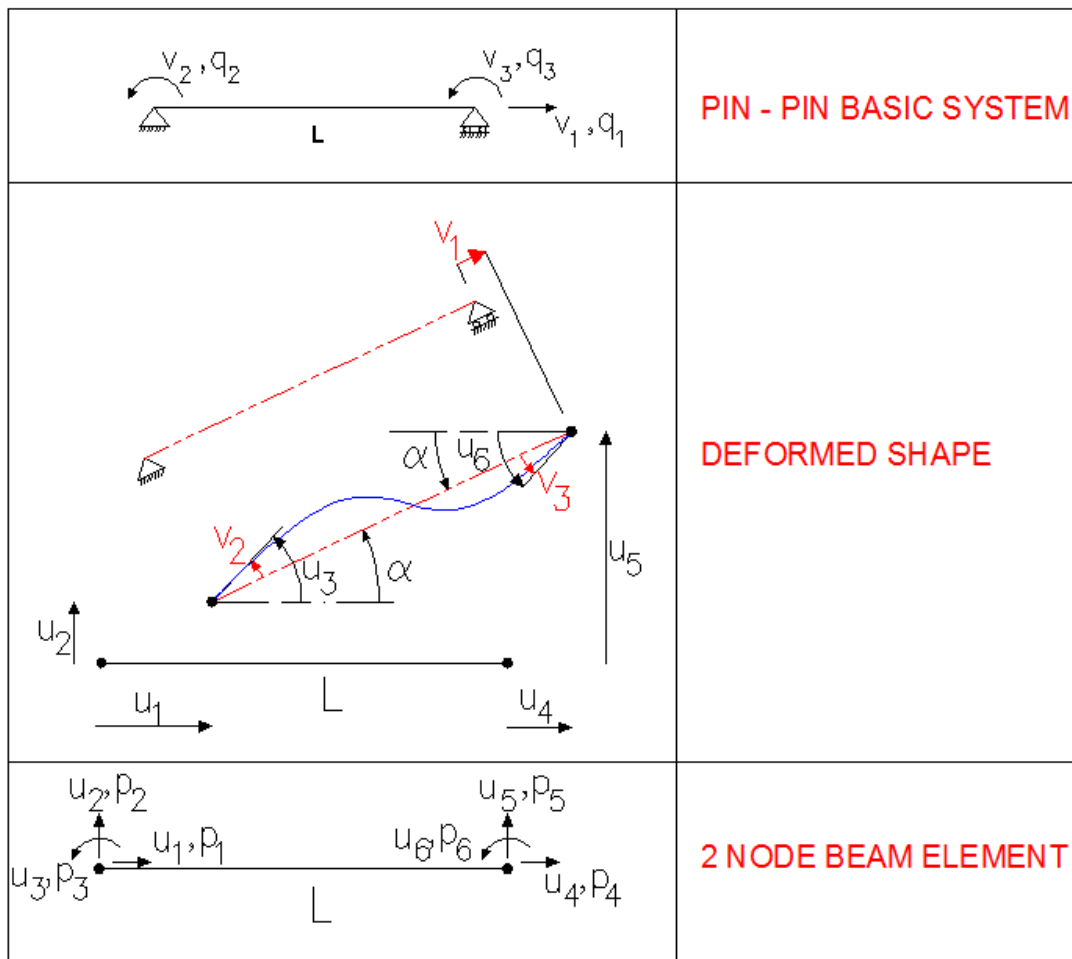


Figure 8 Conversion from simply supported system to 2 node beam element

Equation (2.20) can be written in matrix notation as

$$\begin{Bmatrix} v_1 \\ v_2 \\ v_3 \\ \underline{v} \end{Bmatrix} = \underbrace{\begin{bmatrix} -1 & 0 & 0 & 1 & 0 & 0 \\ 0 & \frac{1}{L} & 1 & 0 & -\frac{1}{L} & 0 \\ 0 & \frac{1}{L} & 0 & 0 & -\frac{1}{L} & 1 \end{bmatrix}}_{\underline{a}} \underbrace{\begin{Bmatrix} u_1 \\ u_2 \\ u_3 \\ u_4 \\ u_5 \\ u_6 \end{Bmatrix}}_{\underline{u}} \quad (2.21)$$

Equilibrium of the basic element forces and the nodal force vector in complete system can be cast as follows:

$$\underbrace{\begin{Bmatrix} p_1 \\ p_2 \\ p_3 \\ p_4 \\ p_5 \\ p_6 \end{Bmatrix}}_{\bar{p}} = \underbrace{\begin{bmatrix} -1 & 0 & 0 \\ 0 & \frac{1}{L} & \frac{1}{L} \\ 0 & 1 & 0 \\ 1 & 0 & 0 \\ 0 & -\frac{1}{L} & -\frac{1}{L} \\ 0 & 0 & 1 \end{bmatrix}}_{a^T} \underbrace{\begin{Bmatrix} q_1 \\ q_2 \\ q_3 \end{Bmatrix}}_q \quad (2.22)$$

Given that basic element forces are related to the basic element deformations with the relation $q = \underline{k}v$, we can substitute (2.21) in (2.22) to get

$$\bar{p} = \underline{k}_{el}u \quad (2.23)$$

where $\underline{k}_{el} = \underline{a}^T \underline{k} \underline{a}$ is the element stiffness matrix in complete system for the two node beam element. This stiffness matrix is actually now calculated in the element local coordinate system. Further transformation can be easily achieved by rotation to the global coordinate system in order to consider the angles between the local coordinates x, y and z and the global coordinates X, Y and Z . In depth discussion of these transformations is available in Filippou and Fenves (2004) for 2d case and Soydas (2013) for 3d case.

2.4. STATE DETERMINATION OF FORCE-BASED ELEMENT

Implementation of the force-based element is sought in standard finite element software that is based on displacement method of analysis. In such a solution platform, displacements are incremented iteratively in order to achieve convergence to the applied loads. Since the force-based element requires the input of element forces and its output is element deformations, an element state determination procedure is necessary for the force-based element to be a part of the solution strategies of displacement-based solutions.

The general procedure for handling nonlinearity in displacement-based finite element solution platform can be summarized as follows. Finite element program solves the nonlinear system of equations between applied forces \underline{P}_{app} and resisting forces \underline{P}_r .

$$\underline{P}_{app} - \underline{P}_r(\underline{u}) \cong \underline{0} \quad (2.24)$$

Since the equation is nonlinear, the system must be linearized in order find the correct displacements that satisfy above equation. By using Taylor's series expansion about an initial guess, an incremental iterative solution for global nodal displacements is obtained as given in the next equation, and this iterative process is also named as Newton-Raphson method.

$$\begin{aligned} \{\underline{P}_{app} - \underline{P}_r(\underline{u}_i)\} - \underbrace{\frac{\partial \underline{P}_r(\underline{u}_i)}{\partial \underline{U}}}_{\underline{K}_i} \Delta \underline{U}_i &= \underline{0} \\ \Delta \underline{U}_i &= \underline{K}_i^{-1} \{\underline{P}_{app} - \underline{P}_r(\underline{u}_i)\} \end{aligned} \quad (2.25)$$

An initial guess for global nodal displacements can be taken as $\underline{U}_0 = \underline{0}$ for the start of analysis or the last state of converged nodal displacements.

After calculation of each increment, global nodal displacements \underline{U} are updated and sent to each element with the purpose of receiving back element forces and stiffness.

Since the force-based element actually provides output of element deformations, then the element state determination can be established by imposing the nodal displacements calculated from Equations (2.21) and (2.25). We denote the imposed element deformations received from the finite element program as $(\hat{\underline{v}})$. Imposed deformations should match with the state of the force-based element, and this compatibility statement can be written as follows:

$$\hat{\underline{v}} - \underline{v}(\underline{q}) \cong \underline{0} \quad (2.26)$$

The term $\underline{v}(q)$ in (2.26) is the response of the force-based element, and under general case the response of the element is nonlinear and requires linearization as written in the next equation:

$$\widehat{\underline{v}} - \left[\underline{v}(q_0) + \underbrace{\frac{\partial \underline{v}}{\partial q}}_{f_0} \bigg|_{q=q_0} \underbrace{(q - q_0)}_{\Delta q} \right] = \underline{0} \quad (2.27)$$

$$\Delta \underline{q} = \left[\underline{f}^i \right]^{-1} \{ \widehat{\underline{v}} - \underline{v}_i \} \quad (2.28)$$

$$q_{i+1} = q_i + \Delta q \quad (2.29)$$

In (2.28) the term inverse of section flexibility matrix $\left[\underline{f}_s^i \right]^{-1}$, that is equal to section stiffness matrix \underline{k}_s , can be computed from (2.17).

With the calculation of new updates for basic element forces from Equation (2.29), new values of section forces can be obtained by the use of Equation (2.2), i.e. $\underline{s}(x) = \underline{b}(x)q$. Since the section state determination requires the input of section deformations but not the section forces, then one more effort is necessary to match the imposed section forces calculated from $\underline{s}(x) = \underline{b}(x)q$ with $\underline{s}(\underline{e})$. For this effort, the imposed section forces are denoted with a hat value to signify the imposed quantity, the equality to be satisfied is written as follows:

$$\widehat{\underline{s}} - \underline{s}(\underline{e}) \cong \underline{0} \quad (2.30)$$

The section deformations must be compatible with element end forces. The term $\underline{s}(\underline{e})$ will be linearized as follows

$$\hat{\underline{s}} - \left[\underline{s}(e_0) + \underbrace{\frac{\partial \underline{s}}{\partial e}}_{\underline{k}_s^0} \underbrace{(e - e_0)}_{\Delta e} \right] = \underline{0} \quad (2.31)$$

Inserting $\hat{\underline{s}} = \underline{b}(x)q$ into (2.31), we get

$$\Delta e = [\underline{k}_s^i]^{-1} \{ \underline{b}(x)q - \underline{s}(e_i) \} \quad (2.32)$$

$$e_{i+1} = e_i + \Delta e \quad (2.33)$$

The element deformations will be computed as given in Equation (2.5) and with the new values of section deformations computed from Equation (2.33), we obtain

$$\underline{v}_{i+1} = \int_0^L \underline{b}^T(x) e_{i+1}(x) dx \quad (2.34)$$

Equation (2.32) requires the calculation of section stiffness matrix \underline{k}_s . The numerical computation process of \underline{k}_s for beams consisting of only one material can be summarized as follows. The material subroutine reads the section deformations (e_{i+1}) and history variables (in case of hardening) at each layer of the beam section and at each integration point along the length of the beam as input, then it takes out the consistent tangent modulus and stresses as output variables. The consistent tangent modulus and stresses at each layer of the beam's cross section are transferred into a numerical integration process to acquire the section stiffness matrix and section forces as written in the following equation:

$$\underline{k}_s = \int_A \underline{a}_s^T \frac{\partial \underline{\sigma}}{\partial \underline{\varepsilon}} \underline{a}_s dA \quad (2.35)$$

For beams with FGM, the section deformations and history variables are sent to two different material subroutines separately and then these two separate material outputs are added in accordance with their weighted material ratio at the layer.

With the calculation of section stiffness matrix, the element flexibility matrices (\underline{f}) and element stiffness matrices (\underline{k}) will also be updated with the use of following equations:

$$\begin{aligned} \underline{f}^{i+1} &= \int_0^L \underline{b}^T(x) \underline{f}_s^{i+1} \underline{b}(x) dx \\ \underline{k}^{i+1} &= [\underline{f}^{i+1}]^{-1} \end{aligned} \quad (2.36)$$

where $\underline{f}_s^{i+1} = [\underline{k}_s^{i+1}]^{-1}$ is the section flexibility matrix corresponding to $\underline{e}_{i+1}(x)$ each section deformations.

The convergence check is handled at the global level through the satisfaction of equilibrium equations within a tolerance, i.e. $\| \underline{P}_{app} - \underline{P}_r(\underline{u}_i) \| < TOLERANCE$, the iteration stops.

2.5. THE CONVERGENCE RATE OF NEWTON–RAPHSON METHOD

Newton–Raphson iteration procedure is utilized for the solution strategy of the nonlinear system of equations. The stiffness matrix is updated and its inverse is calculated at each iteration. As exhausting as it may seem in terms of computational cost, the convergence rate of this method is quite powerful.

The convergence rate of the Newton–Raphson method can be proven as follows. First the Taylor series will be portrayed

$$f(\alpha) = f(x_n) + \frac{f'(x_n)(\alpha - x_n)}{1!} + \underbrace{\frac{f''(x_n)(\alpha - x_n)^2}{2!} + \frac{f^{(3)}(x_n)(\alpha - x_n)^3}{3!} + \dots}_{\text{Higher Order Terms (H.O.T.)}} = 0 \quad (2.37)$$

Making use of the mean value theorem, one can prove the existence of such point $x = \xi$ that satisfies (2.37) in the following form

$$f(\alpha) = f(x_n) + \frac{f'(x_n)(\alpha - x_n)}{1!} + \frac{f''(\xi)(\alpha - x_n)^2}{2!} = 0 \quad (2.38)$$

In (2.38), $\frac{f''(\xi)(\alpha - x_n)^2}{2!}$ represents the H.O.T. (higher order terms).

The iteration steps of Newton–Raphson method is visualized in Figure 9

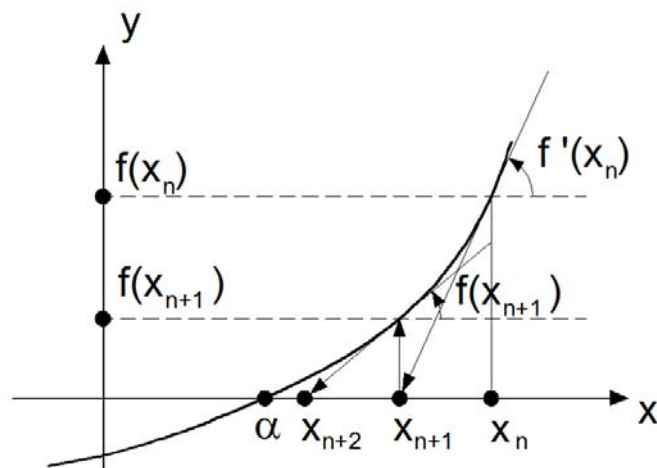


Figure 9 Visualization of Newton–Raphson iterations

Following relation can be comprised from Figure 9

$$x_{n+1} = x_n - \frac{f(x_n)}{f'(x_n)} \quad (2.39)$$

After dividing (2.38) with $f'(x_n)$ and rearranging the terms, the following equation is obtained

$$\left[\frac{f(x_n)}{f'(x_n)} - x_n \right] + \alpha + \frac{f''(\xi)(\alpha - x_n)^2}{2f'(x_n)} = 0 \quad (2.40)$$

Inserting (2.39) into (2.40) leads us to the final relation between the error terms of successive iterations.

$$\underbrace{\alpha - x_{n+1}}_{\varepsilon_{n+1}} = \frac{-f''(\xi)}{2f'(x_n)} \underbrace{(\alpha - x_n)^2}_{\varepsilon_n^2} \quad (2.41)$$

Taking the absolute of right and left sides, we can write

$$|\varepsilon_{n+1}| = \left| \frac{f''(\xi)}{2f'(x_n)} \right| (\varepsilon_n)^2 \quad (2.42)$$

Since there is a quadratic relation between the errors of successive iterations, the convergence rate of Newton–Raphson iteration method is quadratic provided that the tangent to the function is accurately calculated.

2.6. FORCE-BASED CONSISTENT MASS MATRIX

In this thesis, mass matrix of the proposed element for FGM beams is obtained in a consistent manner with the formulation of the element. Since the proposed element does not require the use of displacement interpolation functions, it is necessary to derive the displacement field along the length of the beam in a consistent way with the force-based formulation. This can actually be obtained in a simple fashion with unit dummy load method, i.e. with the use of principle of virtual forces approach as done in the derivation of the element in Section 2.1. Such an approach was proposed by Molins et al. (1998) and successfully implemented and used recently by Soydas (2013). With this alternative derivation of consistent mass matrix, we can obtain the mass matrix of any type of beam element that is uniform or tapered and with homogeneous or heterogeneous material distribution.

Derivation of the mass matrix within force-based approach relies on the use of cantilever basic system due to its simplicity in establishing the displacement field. For the cantilever basic system, the basic element forces are axial force and

transverse (shear) force and moment values at the right node, while the left node is fixed. Actually these three basic forces exactly match with the element end forces for the complete system as well. Denoting the basic forces of cantilever system as \underline{q}_c , we can calculate the section forces as follows:

$$\underline{s}(x) = \begin{Bmatrix} N(x) \\ V(x) \\ M(x) \end{Bmatrix} = \underline{b}_c(x, L) \underline{q}_c \quad (2.43)$$

Where the section forces are arranged as given above, and the force interpolation matrix for the cantilever basic system is

$$\underline{b}_c(x, L) = \begin{bmatrix} 1 & 0 & 0 \\ 0 & 1 & 0 \\ 0 & (L-x) & 1 \end{bmatrix} \quad (2.44)$$

The section mass and stiffness matrices are calculated as:

$$\underline{m}_s(x) = \int_A \underline{a}_s^T \rho(y) \underline{a}_s dA \quad (2.45)$$

$$\underline{k}_s(x) = \int_A \underline{a}_s^T \begin{bmatrix} E(y) & 0 \\ 0 & G(y) \end{bmatrix} \underline{a}_s dA \quad (2.46)$$

where \underline{a}_s the section compatibility matrix previously introduced in Equations (2.10) and (2.11) is rearranged as follows:

$$\underline{a}_s = \begin{bmatrix} 1 & 0 & -y \\ 0 & 1 & 0 \end{bmatrix} \quad (2.47)$$

Mass matrix of the force-based element is written in a 6×6 dimension, i.e. in the complete system with 3 degrees of freedom per each end node, as follows:

$$\underline{m}_{el} = \begin{bmatrix} \underline{m}_{11} & \underline{m}_{12} \\ \underline{m}_{21} & \underline{m}_{22} \end{bmatrix} \quad (2.48)$$

Where the components of element mass matrix are calculated from sub-matrices

$$\underline{m}_{22} = \underline{f}_c^{-1} \int_0^L \underline{b}_c^T(x, L) \underline{k}_s^{-1}(x) \left(\int_x^L \underline{b}_c^T(x, \xi) \underline{m}_s(\xi) \underline{f}_{cp}(\xi) \underline{f}_c^{-1} d\xi \right) dx \quad (2.49)$$

$$\underline{m}_{21} = \underline{f}_c^{-1} \int_0^L \underline{b}_c^T(x, L) \underline{k}_s^{-1}(x) \left(\int_x^L \underline{b}_c^T(x, \xi) \underline{m}_s(\xi) \left(\underline{b}_c^T(0, \xi) - \underline{f}_{cp}(\xi) \underline{f}_c^{-1} \underline{b}_c^T(0, L) \right) d\xi \right) dx \quad (2.50)$$

$$\underline{m}_{12} = \underline{m}_{21} = -\underline{b}_c(0, L) \underline{m}_{22} + \int_0^L \underline{b}_c(0, x) \underline{m}_s(x) \underline{f}_{cp}(x) \underline{f}_c^{-1} dx \quad (2.51)$$

$$\underline{m}_{11} = -\underline{b}_c(0, L) \underline{m}_{21} + \int_0^L \underline{b}_c(0, x) \underline{m}_s(x) \left(\underline{b}_c^T(0, x) - \underline{f}_{cp}(x) \underline{f}_c^{-1} \underline{b}_c^T(0, L) \right) dx \quad (2.52)$$

In above equations, element flexibility matrix for the cantilever system is denoted as \underline{f}_c , and it is calculated as follows:

$$\underline{f}_c = \int_0^L \underline{b}_c^T(x, L) \underline{k}_s^{-1}(x) \underline{b}_c(x, L) dx \quad (2.53)$$

And the partial flexibility matrix \underline{f}_{cp} of the cantilever system is given as:

$$\underline{f}_{cp}(x) = \int_0^x \underline{b}_c^T(\xi, x) \underline{k}_s^{-1}(\xi) \underline{b}_c(\xi, x) d\xi \quad (2.54)$$

Force-based consistent mass matrix for prismatic beams with FGM obtained from Equations (2.48) to (2.53) are compared with the mass matrix of the displacement-based element proposed by Chakraborty et al. (2003) that is presented in the next chapter, and they are observed to be giving the same matrix for uniform prismatic FGM beams. However, in the case when the beam is tapered, then the displacement-based approach will result in an approximation, while the proposed approach will still give the exact consistent mass matrix for FGM beams.

CHAPTER 3

A DISPLACEMENT-BASED ELEMENT FOR FGM BEAMS

In this chapter, a previously developed beam finite element for FGM Chakraborty et al. (2003) will be discussed. Some of the formulations and derivation steps that have not been clearly stated in Chakraborty et al. (2003) are presented in detail.

Also, during this investigation, it has also been detected that a coefficient used in shape functions appears to be represented incorrectly. Since the mentioned finite beam element will be used in the numerical examples and verifications, the presentation of this element is justified for the sake of completeness.

3.1. FORMULATION OF DISPLACEMENT-BASED ELEMENT

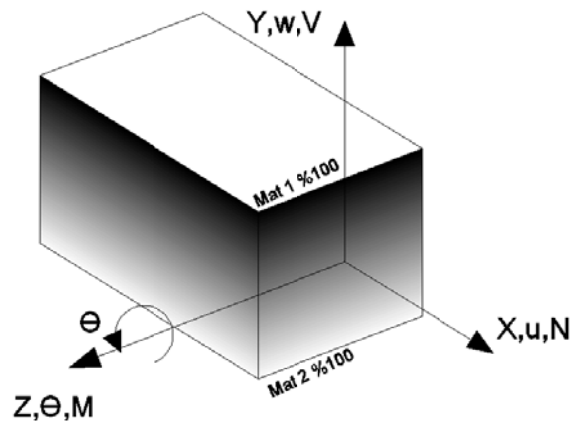


Figure 10 Coordinate system for the finite element model

In Chakraborty et al. (2003), considering Timoshenko beam theory, the axial and transverse displacement fields are expressed as,

$$\begin{aligned} U(x, y, z, t) &= u(x, t) - y\phi(x, t) \\ W(x, y, z, t) &= w(x, t) \end{aligned} \quad (3.1)$$

The strains are expressed as

$$\begin{aligned} \varepsilon_x &= \frac{\partial U}{\partial x} = u_{,x} - y\phi_{,x} \\ \gamma_{xy} &= \frac{\partial U}{\partial y} + \frac{\partial W}{\partial x} = -\phi + w_{,x} \end{aligned} \quad (3.2)$$

Where $(.)_{,x}$ represents differentiation with respect to x-axis.

The relation between stress and strain is expressed as

$$\begin{Bmatrix} \sigma_x \\ \tau_{xy} \end{Bmatrix} = \begin{bmatrix} E(y) & 0 \\ 0 & G(y) \end{bmatrix} \begin{Bmatrix} \varepsilon_x \\ \gamma_{xy} \end{Bmatrix} \quad (3.3)$$

The strain energy (S) and kinetic energy (T) are written as

$$S = \frac{1}{2} \int_0^L \int_A (\sigma_x \varepsilon_x + \tau_{xy} \gamma_{xy}) dA dx \quad (3.4)$$

$$T = \frac{1}{2} \int_0^L \int_A \rho(y) (\dot{U}^2 + \dot{W}^2) dA dx \quad (3.5)$$

Where $(\dot{})$ represents the time derivative. $\rho(y)$, L and A are density, length and the area of the cross section. Applying Hamilton's principle, the following equations of motion are obtained. The implementation of Hamilton's principle is explained in Appendix.

$$\begin{aligned} \delta u : I_0 \ddot{u} - I_1 \ddot{\phi} - A_{11} u_{,xx} + B_{11} \phi_{,xx} &= 0 \\ \delta w : I_0 \ddot{w} - A_{55} (w_{,xx} - \phi_{,x}) &= 0 \\ \delta \phi : I_2 \ddot{\phi} - I_1 \ddot{u} + B_{11} u_{,xx} - D_{11} \phi_{,xx} - A_{55} (w_{,x} - \phi) &= 0 \end{aligned} \quad (3.6)$$

Where

$$\begin{aligned}
[A_{11} \quad B_{11} \quad D_{11}] &= \int_A [1 \quad y \quad y^2] E(y) dA \\
A_{55} &= \int_A G(y) dA \\
[I_0 \quad I_1 \quad I_2] &= \int_A [1 \quad y \quad y^2] \rho(y) dA
\end{aligned} \tag{3.7}$$

The interpolation functions for u, w, ϕ are selected for the element to be giving a shear-locking free element.

In case of assigning interpolation functions improperly for the vertical translation and slope, the phenomenon called shear locking occurs. Especially, if linear interpolation functions are assigned for both vertical translation and slope, then the beam element behaves very stiff for larger values of length to depth ratio. To deal with this phenomenon, one should use higher order interpolation functions for vertical translation than slope.

Since the order of interpolation function for vertical translation (w) is higher than the order of the interpolation function for the slope (ϕ) as discussed by Reddy (1997).

$$\begin{aligned}
u &= c_1 + c_2 x + c_3 x^2 \\
w &= c_4 + c_5 x + c_6 x^2 + c_7 x^3 \\
\phi &= c_8 + c_9 x + c_{10} x^2
\end{aligned} \tag{3.8}$$

The term B_{11} and I_1 is zero for homogenous sections. Completing the following formulations with the specified shape in such case will end up with the stiffness matrix in Reddy (1997), i.e. the Interdependent Interpolation Element for Timoshenko's beam theory. This so called beam element is been utilized as the default frame element for some popular FEM packages like SAP2000.

Equation (3.8) is substituted into the static part of (3.6). The static part of (3.6) is obtained by eliminating the terms with time derivatives, thus the governing partial differential equation is transformed into a system of ordinary differential equations.

The static part of (3.6) can be shown as

$$\delta u : -A_{11}u_{,xx} + B_{11}\phi_{,xx} = 0 \dots\dots\dots(3.13.1)$$

$$\delta w : -A_{55}(w_{,xx} - \phi_{,x}) = 0 \dots\dots\dots(3.13.2) \quad (3.9)$$

$$\delta \phi : B_{11}u_{,xx} - D_{11}\phi_{,xx} - A_{55}(w_{,x} - \phi) \dots\dots(3.13.3)$$

Also

$$\begin{bmatrix} u_{,xx} \\ w_{,x} \\ w_{,xx} \\ \phi_{,x} \\ \phi_{,xx} \end{bmatrix} = \begin{bmatrix} 2c_3 \\ c_5 + 2c_6x + 3c_7x^2 \\ 2c_6 + 6c_7x \\ c_9 + 2c_{10} \\ 2c_{10} \end{bmatrix} \quad (3.10)$$

Substituting (3.10) into (3.9)₁

$$c_3 = c_{10} \frac{B_{11}}{A_{11}} \quad (3.11)$$

Substituting (3.10) into (3.9)₂

$$2c_6 + 6c_7x - c_9 - 2c_{10}x = 0 \quad (3.12)$$

From (3.12)

$$\begin{aligned} c_7 &= \frac{c_{10}}{3} \\ c_6 &= \frac{c_9}{2} \end{aligned} \quad (3.13)$$

Substituting (3.10) into (3.9)₂ and using (3.11)

$$\begin{aligned} 2B_{11}c_3 - 2D_{11}c_{10} - A_{55}(c_5 + 2c_6x + 3c_7x^2 - c_8 - c_9x - c_{10}x^2) &= 0 \\ 2B_{11}c_3 - 2D_{11}c_{10} - A_{55}(c_5 - c_8) &= 0 \\ 2\frac{B_{11}^2}{A_{11}}c_{10} - 2D_{11}c_{10} - A_{55}(c_5 - c_8) &= 0 \\ c_{10} &= -\beta(c_5 - c_8)/2 \\ c_3 &= \alpha(c_5 - c_8)/2 \end{aligned} \quad (3.14)$$

Where $\beta = \frac{A_{11}A_{55}}{(B_{11}^2 - D_{11}A_{11})}$ and $\alpha = \frac{B_{11}A_{55}}{(B_{11}^2 - D_{11}A_{11})}$

Using (3.13) and (3.14) interpolation functions can be rewritten as

$$\begin{aligned} u &= c_1 + c_2x + \frac{1}{2}\alpha(c_5 - c_8)x^2 \\ w &= c_4 + c_5x + \frac{1}{2}c_9x^2 - \frac{1}{6}\beta(c_5 - c_8)x^3 \\ \phi &= c_8 + c_9x - \frac{1}{2}\beta(c_5 - c_8)x^2 \end{aligned} \quad (3.15)$$

In matrix form

$$\begin{aligned} \{u\} &= \begin{bmatrix} u \\ w \\ \phi \end{bmatrix} = [N(x)]\{a\} \\ \{a\} &= \{c_1, c_2, c_4, c_5, c_8, c_9\} \end{aligned} \quad (3.16)$$

A relation can be formed between column vector $\{a\}$ and nodal displacements by using boundary conditions for each node, (at $x=0$ and $x=L$)

$$\begin{aligned} [G]^{-1} &= \begin{bmatrix} N(0) \\ N(L) \end{bmatrix} \\ \{\hat{u}\} &= [G]^{-1}\{a\} \\ \{a\} &= [G]\{\hat{u}\} \end{aligned} \quad (3.17)$$

Where $[N(x)]$, $[G]^{-1}$ and $[G]$ are

$$[N(x)] = \begin{bmatrix} 1 & x & 0 & -\frac{1}{2}\alpha x^2 & \frac{1}{2}\alpha x^2 & 0 \\ 0 & 0 & 1 & x - \frac{1}{6}\beta x^3 & \frac{1}{6}\beta x^3 & \frac{1}{2}x^2 \\ 0 & 0 & 0 & -\frac{1}{2}\beta x^2 & 1 + \frac{1}{2}\beta x^2 & x \end{bmatrix} \quad (3.18)$$

$$[G]^{-1} = \begin{bmatrix} 1 & 0 & 0 & 0 & 0 & 0 \\ 0 & 0 & 1 & 0 & 0 & 0 \\ 0 & 0 & 0 & 0 & 1 & 0 \\ 1 & L & 0 & -\frac{1}{2}\alpha L^2 & \frac{1}{2}\alpha L^2 & 0 \\ 0 & 0 & 1 & L - \frac{1}{6}\beta L^3 & \frac{1}{6}\beta L^3 & \frac{1}{2}L^2 \\ 0 & 0 & 0 & -\frac{1}{2}\beta L^2 & 1 + \frac{1}{2}\beta L^2 & L \end{bmatrix} \quad (3.19)$$

$$[G] = \begin{bmatrix} 1 & 0 & 0 & 0 & 0 & 0 \\ -\frac{1}{L} & \frac{-6\alpha}{\beta L^2 + 12} & \frac{-3\alpha L}{\beta L^2 + 12} & \frac{1}{L} & \frac{6\alpha}{\beta L^2 + 12} & \frac{-3\alpha L}{\beta L^2 + 12} \\ 0 & 1 & 0 & 0 & 0 & 0 \\ 0 & \frac{-12}{\beta L^3 + 12L} & \frac{\beta L^2 + 6}{\beta L^2 + 12} & 0 & \frac{12}{\beta L^3 + 12L} & \frac{-6}{\beta L^2 + 12} \\ 0 & 0 & 1 & 0 & 0 & 0 \\ 0 & \frac{-6\beta}{\beta L^2 + 12} & \frac{-(4\beta L^2 + 12)}{\beta L^3 + 12L} & 0 & \frac{6\beta}{\beta L^2 + 12} & \frac{-(2\beta L^2 - 12)}{\beta L^3 + 12L} \end{bmatrix} \quad (3.20)$$

$\{\hat{u}\} = \{u_1 \quad w_1 \quad \phi_1 \quad u_2 \quad w_2 \quad \phi_2\}^T$ is the vector of nodal displacements of the element.

The exact shape functions can be derived by multiplying $[N(x)]$ and $[G]$

$$\begin{aligned} \begin{Bmatrix} u \\ w \\ \phi \end{Bmatrix} &= [N(x)]\{a\} = [N(x)][G]\{\hat{u}\} = [\aleph(x)]\{\hat{u}\} \\ [\aleph(x)] &= [N(x)][G] \end{aligned} \quad (3.21)$$

$[\aleph(x)] = [\aleph_u(x) \quad \aleph_w(x) \quad \aleph_\phi(x)]^T$ is a 3x6 matrix containing the exact shape functions for axial, transverse and rotational degrees of freedom.

Element force members (axial, shear and moment) can be expressed as

$$\begin{aligned}
N_x &= \int_A \sigma_{xx} dA \\
V_x &= \int_A \tau_{xx} dA \\
M_x &= \int_A -y \sigma_{xx} dA
\end{aligned} \tag{3.22}$$

Imposing (3.2) and (3.3); (3.22) can be written as

$$\begin{aligned}
N_x &= A_{11}u_{,x} - B_{11}\phi_{,x} \\
V_x &= A_{55}(w_{,x} - \phi) \\
M_x &= -B_{11}u_{,x} + D_{11}\phi_{,x}
\end{aligned} \tag{3.23}$$

From (3.23) element force vector can be associated with vector $\{a\}$ in matrix form as

$$\{F\} = [\bar{G}]\{a\} \tag{3.24}$$

where $[\bar{G}]$ and $\{F\}$ are

$$[\bar{G}] = \begin{bmatrix} 0 & -A_{11} & 0 & 0 & 0 & B_{11} \\ 0 & 0 & 0 & -A_{55} & A_{55} & 0 \\ 0 & B_{11} & 0 & 0 & 0 & -D_{11} \\ 0 & A_{11} & 0 & 0 & 0 & -B_{11} \\ 0 & 0 & 0 & A_{55} & -A_{55} & 0 \\ 0 & -B_{11} & 0 & (\alpha B_{11} - \beta D_{11})L & (\beta D_{11} - \alpha B_{11})L & D_{11} \end{bmatrix} \tag{3.25}$$

$$\{F\} = [-N_x(0) \quad -V_x(0) \quad -M_x(0) \quad N_x(L) \quad V_x(L) \quad M_x(L)] \tag{3.26}$$

The stiffness matrix can be evaluated by substituting (3.17) into (3.24)

$$\{F\} = [\bar{G}][G]\{\hat{u}\} = [K]\{\hat{u}\} \tag{3.27}$$

$[N(x)]$ (exact shape functions) and $[K]$ (stiffness matrix) are

$$[S(x)] = \begin{bmatrix} 1 - \frac{x}{L} & 0 & 0 \\ 6\alpha\psi x \left(\frac{x}{L} - 1\right) & \frac{\psi(\beta L^3 + 12L - 12x + 2\beta x^3 - 3\beta x^2 L)}{L} & 6x\beta\psi \left(\frac{x}{L} - 1\right) \\ 3\alpha\psi x L \left(\frac{x}{L} - 1\right) & \frac{x\psi(\beta L^3 + 6L - 6x + \beta x^2 L - 2\beta x L^2)}{L} & \frac{\psi(3\beta x^2 L + \beta L^3 + 12L - 4x\beta L^2 - 12x)}{L} \\ \frac{x}{L} & 0 & 0 \\ -6\alpha\psi x \left(\frac{x}{L} - 1\right) & \frac{-x\psi(-12 + 2\beta x^2 - 3\beta x L)}{L} & -6x\beta\psi \left(\frac{x}{L} - 1\right) \\ 3\alpha\psi x L \left(\frac{x}{L} - 1\right) & \frac{x\psi(-6L + \beta x^2 L - \beta x L^2 + 6x)}{L} & \frac{x\psi(3\beta x L - 2\beta L^2 + 12)}{L} \end{bmatrix} \quad (3.28)$$

$$[K] = \begin{bmatrix} A_{11} / L & 0 & -B_{11} / L & -A_{11} / L & 0 & B_{11} / L \\ 0 & \frac{12A_{55}\psi}{L} & 6A_{55}\psi & 0 & -\frac{12A_{55}\psi}{L} & 6A_{55}\psi \\ -B_{11} / L & 6A_{55}\psi & \frac{D_{11}}{L} + 3A_{55}\psi L & B_{11} / L & -6A_{55}\psi & -\frac{D_{11}}{L} + 3A_{55}\psi L \\ -A_{11} / L & 0 & B_{11} / L & A_{11} / L & 0 & -B_{11} / L \\ 0 & -\frac{12A_{55}\psi}{L} & -6A_{55}\psi & 0 & \frac{12A_{55}\psi}{L} & 6A_{55}\psi \\ B_{11} / L & 6A_{55}\psi & -\frac{D_{11}}{L} + 3A_{55}\psi L & -B_{11} / L & 6A_{55}\psi & \frac{D_{11}}{L} - 3A_{55}\psi L \end{bmatrix} \quad (3.29)$$

where $\psi = \frac{1}{12 + \beta L^2}$

3.2. THE CONSISTENT MASS MATRIX

The consistent mass matrix is described as summation of four sub-matrices as given by Chakraborty et al. (2003).

$$[M] = [M_u] + [M_w] + [M_\phi] + [M_{u\phi}] \quad (3.30)$$

$[M_u]$, $[M_w]$ and $[M_\phi]$ stand for the contributions of axial (u), translational (w) and slope (ϕ) degree of freedoms. $[M_{u\phi}]$ represents the coupling between axial and slope degree of freedoms.

The components of consistent mass matrix are figured as follows

$$\begin{aligned}
 [M_u] &= \int_0^L I_0 ([\mathfrak{N}_u]^T [\mathfrak{N}_u]) dx \\
 [M_w] &= \int_0^L I_0 ([\mathfrak{N}_w]^T [\mathfrak{N}_w]) dx \\
 [M_\phi] &= \int_0^L I_2 ([\mathfrak{N}_\phi]^T [\mathfrak{N}_\phi]) dx \\
 [M_{u\phi}] &= -\int_0^L I_1 ([\mathfrak{N}_u]^T [\mathfrak{N}_\phi] + [\mathfrak{N}_\phi]^T [\mathfrak{N}_u]) dx
 \end{aligned} \tag{3.31}$$

For homogenous sections; since I_1 is zero, it can be indicated from (3.31) that the term $[M_{u\phi}]$ yields zero.

CHAPTER 4

MODELING INELASTIC BEHAVIOR OF FGM BEAMS

In this chapter, firstly the von Mises plasticity and its yield criteria will be presented. Secondly, evolution equations will be derived for the von Mises model with linear kinematic and linear isotropic hardening. Finally the stress update algorithm for hardening plasticity will be indicated.

Generally, von Mises plasticity model is used for modeling the inelastic behavior of metals. For nonlinear analyses of beams with functionally graded materials the use of the von Mises plasticity for metallic part and Drucker-Prager plasticity model for ceramic part of FGM is suggested in Bocciarelli et al. (2008). Despite this suggestion, as a first effort to the analysis of FGM beams, inelastic analyses carried out in Chapter 5 will use the same material model for both metallic and ceramic parts; since it is observed that the degree of material change can actually ensure such a choice is valid as long as one of the materials state of stress allows such a use. Detailed explanation will be presented in Chapter 5.

With such a choice, von Mises plasticity model is adopted for describing the inelastic behavior of both constituting parts of FGM.

4.1. VON MISES PLASTICITY

In solid mechanics, the stress tensor can be divided into two parts. These are called as the volumetric part and the deviatoric part. The volumetric part does not involve yielding for the von Mises plasticity since it is only related with the first invariant.

Only the deviatoric part can provoke yielding. So the following decomposition is considered

$$\underline{\sigma} = \frac{1}{3}tr(\underline{\sigma})\underline{1} + dev(\underline{\sigma}) = p\underline{1} + \underline{\sigma}' \quad (4.1)$$

Where $p = \frac{1}{3}tr(\underline{\sigma})$ and $\underline{\sigma}' = dev(\underline{\sigma})$.

The J_2 – invariant of $\underline{\sigma}' = dev(\underline{\sigma})$ is introduced

$$J_2 = \frac{1}{2}tr[\underline{\sigma}'\underline{\sigma}'] = \frac{1}{2}\underline{\sigma}' : \underline{\sigma}' \quad (4.2)$$

Assuming that the material is under such uniaxial stress $\underline{\sigma}_u = \begin{bmatrix} \sigma_{11} & 0 & 0 \\ 0 & 0 & 0 \\ 0 & 0 & 0 \end{bmatrix}$ and the

yielding starts at $\sigma_{11} = y_0$. As mentioned above, deviatoric stresses cause yielding for von Mises plasticity. Starting from this argument, the norm of $\underline{\sigma}_u @ (\sigma_{11} = y_0)$ and the norm of the applied stress is compared, and we get

$$\|dev(\underline{\sigma}_u)\| = \left\| \begin{bmatrix} \frac{2}{3}y_0 & 0 & 0 \\ 0 & -\frac{1}{3}y_0 & 0 \\ 0 & 0 & -\frac{1}{3}y_0 \end{bmatrix} \right\| = \sqrt{\frac{2}{3}}y_0$$

Thus, the von Mises theory of plasticity assumes the following yield function.

$$\Phi(\underline{\sigma}') = \sqrt{\underline{\sigma}' : \underline{\sigma}'} - \sqrt{\frac{2}{3}}y_0 = \|\underline{\sigma}'\| - \sqrt{\frac{2}{3}}y_0 \leq 0 \quad (4.3)$$

The spectral decomposition of $\underline{\sigma}$ is considered as

$$\underline{\sigma} = \sum_{i=1}^3 \sigma_i (\underline{n}_i \otimes \underline{n}_i) \quad (4.4)$$

In Figure 11 the visualization of the von Mises yield surface $\Phi = 0$ in the principal stress space is shown. The yield surface corresponds to a cylinder with an axis coincident with the hydrostatic stress state, i.e. $\sigma_1 = \sigma_2 = \sigma_3$

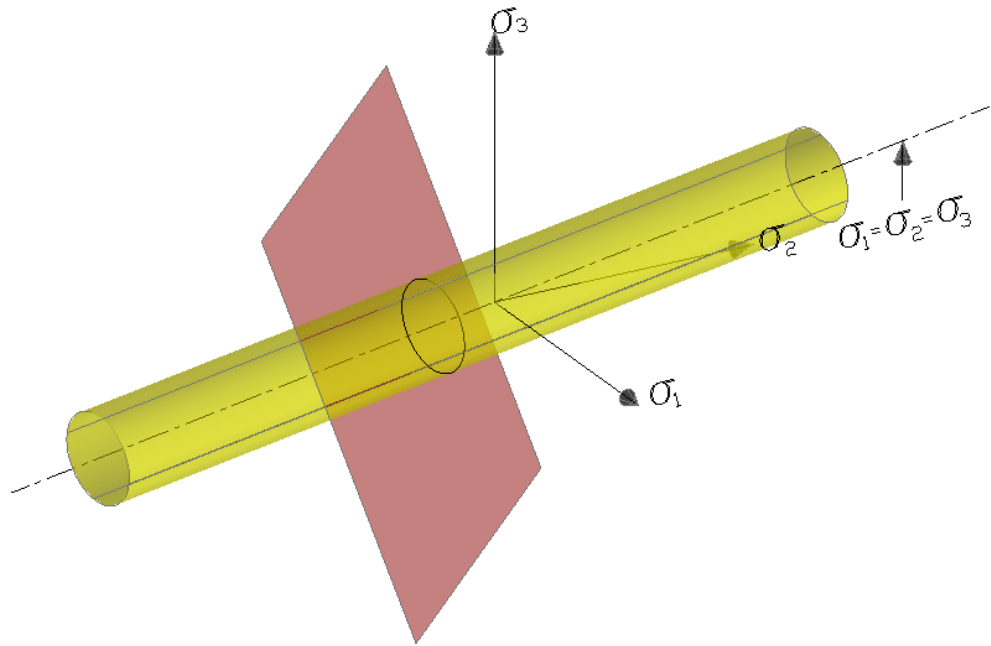


Figure 11 Visualization of the von Mises yield surface

4.2. VON MISES PLASTICITY WITH LINEAR ISOTROPIC AND KINEMATIC HARDENING

A basic model problem of J2-plasticity with a combined isotropic and kinematic hardening is considered. The state of the material is described by $\{\underline{\varepsilon}, \underline{\varepsilon}^p, \underline{\alpha}, \alpha\}$, where $\underline{\varepsilon}, \underline{\varepsilon}^p, \underline{\alpha}$ and α are total strain, plastic strain, internal variable for kinematic hardening and internal variable for isotropic hardening, respectively.

The free energy function is assumed to have the following form

$$\psi = \psi^e(\underline{\varepsilon} - \underline{\varepsilon}^p) + \psi^p(\underline{\alpha}, \alpha) \quad (4.5)$$

where $\underline{\varepsilon}^e = \underline{\varepsilon} - \underline{\varepsilon}^p$. The particular form of the free energy function is chosen as

$$\psi = \underbrace{\frac{1}{2}\kappa(e^e)^2 + \mu\underline{\varepsilon}^e : \underline{\varepsilon}^e}_{\psi^e} + \underbrace{\frac{1}{2}h\alpha^2 + \frac{1}{2}H\underline{\alpha} : \underline{\alpha}}_{\psi^p} \quad (4.6)$$

In (4.6) κ , μ , H and h are bulk modulus, shear modulus, linear kinematic hardening parameter and linear isotropic hardening parameter, respectively, with $e^e = \text{tr}(\underline{\varepsilon}^e)$.

Stresses are obtained from (4.6) as follows

$$\underline{\sigma} = \partial_{\underline{\varepsilon}^e} \psi = \kappa e^e \underline{1} + 2\mu \underline{\varepsilon}^e \quad (4.7)$$

Thermodynamical forces $\underline{\beta}, \beta$ conjugate to internal variables $\underline{\alpha}, \alpha$ are obtained as

$$\underline{\beta} = \partial_{\underline{\alpha}} \psi \quad \beta = \partial_{\alpha} \psi \quad (4.8)$$

Evolution equations for $\underline{\varepsilon}^p, \underline{\alpha}$ and α are obtained by a generalization of maximum dissipation. The elastic domain is defined as

$$\mathbb{E} = \{(\underline{\sigma}, \underline{\beta}, \beta) \in R^{3 \times 3} \times R^{3 \times 3} \times R \mid \phi(\underline{\sigma}, \underline{\beta}, \beta) \leq 0\} \quad (4.9)$$

where

$$\begin{aligned} \phi(\underline{\sigma}, \underline{\beta}, \beta) &= \|\underline{\xi}\| - \sqrt{\frac{2}{3}}(y_0 + \beta) \leq 0 \\ \underline{\xi} &= \underline{\sigma}' - \underline{\beta} \end{aligned} \quad (4.10)$$

The boundary of the elastic domain (4.11) defines a yield surface in stress-space.

$$\partial \mathbb{E} = \{(\underline{\sigma}, \underline{\beta}, \beta) \in R^{3 \times 3} \times R^{3 \times 3} \times R \mid \phi(\underline{\sigma}, \underline{\beta}, \beta) = 0\} \quad (4.11)$$

The principle of maximum dissipation states that for a given plastic strain, kinematic hardening parameter and isotropic hardening parameter $\underline{\xi}^p, \underline{\alpha}, \alpha$ among all possible stresses $\underline{\sigma}^*, \underline{\beta}^*, \beta^*$, i.e. $\phi(\underline{\sigma}, \underline{\beta}, \beta) \leq 0$, the plastic dissipation

$$D^* = \underline{\sigma}^* : \underline{\dot{\xi}}^p - \underline{\beta}^* : \underline{\dot{\alpha}} - \beta^* \dot{\alpha} \quad (4.12)$$

attains its maximum.

The actual dissipation is obtained by the following maximization problem

$$\begin{aligned} D &= \text{MAX} \{ \underline{\sigma}^* : \underline{\dot{\xi}}^p - \underline{\beta}^* : \underline{\dot{\alpha}} - \beta^* \dot{\alpha} \} \\ (\underline{\sigma}^*, \underline{\beta}^*, \beta^*) &\in R^{3 \times 3} \times R^{3 \times 3} \times R \end{aligned} \quad (4.13)$$

The maximization problem (4.13) is handled by using the method of Lagrange multipliers. Instead of the maximizing the dissipation under the constraint condition $\phi(\underline{\sigma}, \underline{\beta}, \beta) \leq 0$, $-D = -\underline{\sigma}^* : \underline{\dot{\xi}}^p + \underline{\beta}^* : \underline{\dot{\alpha}} + \beta^* \dot{\alpha}$ will be minimized. The corresponding Lagrange functional is written as follows

$$\mathfrak{L}(\underline{\sigma}, \underline{\beta}, \beta, \lambda) = -\underline{\sigma}^* : \underline{\dot{\xi}}^p + \underline{\beta}^* : \underline{\dot{\alpha}} + \beta^* \dot{\alpha} + \lambda \phi(\underline{\sigma}, \underline{\beta}, \beta) \quad (4.14)$$

Gives the evolution equation

$$\begin{aligned} \underline{\dot{\xi}}^p &= \lambda \partial_{\underline{\sigma}} \phi = \lambda \partial_{\underline{\xi}} \phi = \lambda \frac{\underline{\xi}}{\|\underline{\xi}\|} = \lambda \frac{\underline{\sigma}' - \underline{\beta}}{\|\underline{\sigma}' - \underline{\beta}\|} \\ \underline{\dot{\alpha}} &= -\lambda \partial_{\underline{\beta}} \phi = +\lambda \partial_{\underline{\xi}} \phi = \lambda \frac{\underline{\sigma}' - \underline{\beta}}{\|\underline{\sigma}' - \underline{\beta}\|} \\ \dot{\alpha} &= -\lambda \partial_{\beta} \phi = \lambda \sqrt{\frac{2}{3}} \end{aligned} \quad (4.15)$$

and

$$\lambda \geq 0 \quad \phi \leq 0 \quad \lambda \phi = 0 \quad (4.16)$$

From (4.15) one can conclude that $\underline{\dot{\xi}}^p = \underline{\dot{\alpha}}$

(4.16) is the loading/unloading conditions (also known as the Karush-Kuhn-Tucker conditions).

The mathematical meaning of the Karush-Kuhn-Tucker conditions can be summarized as; either the constraint is active ($\lambda > 0, \phi = 0$) or inactive ($\lambda = 0, \phi < 0$). As well as, the physical meaning of (4.16) states that either plastic flow or unloading occurs.

$$\|\dot{\xi}^p\| = \lambda \|\partial_{\xi} \Phi\| = \lambda \frac{\|\xi\|}{\|\xi\|} = \lambda \quad (4.17)$$

λ indicates a physical property (norm of the rate of change of plastic strain tensor)

The evolution of α (isotropic hardening variable)

$$\dot{\alpha} = \sqrt{\frac{2}{3}} \lambda = \sqrt{\frac{2}{3}} \|\dot{\xi}^p\| = \sqrt{\frac{2}{3}} \sqrt{\dot{\xi}^p : \dot{\xi}^p} \quad (4.18)$$

is directly related to the evolution of plastic strain.

4.3. STRESS UPDATE ALGORITHM FOR HARDENING PLASTICITY

We integrate the evolution equations (4.15) by using an implicit backward Euler Algorithm.

$$\begin{aligned} \xi_{n+1}^p &= \xi_n^p + \gamma_{n+1} \underline{n}_{n+1} \\ \alpha_{n+1} &= \alpha_n + \gamma_{n+1} \underline{n}_{n+1} \\ \alpha_{n+1} &= \alpha_n + \gamma_{n+1} \sqrt{\frac{2}{3}} \end{aligned} \quad (4.19)$$

where $\underline{n}_{n+1} = \frac{\xi_{n+1}^p}{\|\xi_{n+1}^p\|}$ and $\xi_{n+1}^p = \sigma_{n+1} - \beta_{n+1}$ along with $\gamma_{n+1} \geq 0, \phi_{n+1} \leq 0, \lambda_{n+1} \phi_{n+1} = 0$

The internal variables at time $t_n \{ \xi_n^p, \alpha_n, \alpha_n \}$ are known. From (4.7) and (4.8)

$$\begin{aligned}
\sigma'_{n+1} &= 2\mu\xi_{n+1}^{e'} = 2\mu(\xi'_{n+1} - \xi_{n+1}^p) \\
\tilde{\beta}_{n+1} &= H\alpha_{n+1} \\
\beta_{n+1} &= h\alpha_{n+1}
\end{aligned} \tag{4.20}$$

The trial state is defined as

$$\begin{aligned}
\sigma_{n+1}^{trial} &= 2\mu(\xi'_{n+1} - \xi_n^p) \\
\tilde{\beta}_{n+1}^{trial} &= H\alpha_n \\
\beta_{n+1}^{trial} &= h\alpha_n
\end{aligned} \tag{4.21}$$

From (4.19) and (4.21), (4.20) can be rewritten as,

$$\begin{aligned}
\sigma'_{n+1} &= \sigma_{n+1}^{trial} - 2\mu\gamma_{n+1}n_{n+1} \\
\tilde{\beta}_{n+1} &= \tilde{\beta}_{n+1}^{trial} + H\gamma_{n+1}n_{n+1} \\
\beta_{n+1} &= \beta_{n+1}^{trial} + h\gamma_{n+1}\sqrt{\frac{2}{3}}
\end{aligned} \tag{4.22}$$

Using the equations above ξ_{n+1} can be written as follows

$$\xi_{n+1} = \sigma_{n+1}' - \tilde{\beta}_{n+1} = \xi_{n+1}^{trial} - (2\mu + H)\gamma_{n+1}n_{n+1} \tag{4.23}$$

Where $\xi_{n+1}^{trial} = \sigma_{n+1}^{trial} - \tilde{\beta}_{n+1}^{trial}$

Rewriting (4.23)

$$\begin{aligned}
\|\xi_{n+1}\|n_{n+1} &= \|\xi_{n+1}^{trial}\|n_{n+1}^{trial} - (2\mu + H)\gamma_{n+1}n_{n+1} \\
n_{n+1} \left[\|\xi_{n+1}\| + (2\mu + H)\gamma_{n+1} \right] &= n_{n+1}^{trial} \|\xi_{n+1}^{trial}\|
\end{aligned} \tag{4.24}$$

From (4.24) we acquire two important equations. Since μ, H, γ_{n+1} and norm of a 2nd order tensor are always positive the unit tensors, n_{n+1}^{trial} and n_{n+1} , must be equal. Hereupon, rest of the terms in (4.24) should satisfy the equality. Therefore,

$$\begin{aligned} \underline{n}_{n+1} &= \underline{n}_{n+1}^{trial} \\ \|\underline{\xi}_{n+1}\| &= \|\underline{\xi}_{n+1}^{trial}\| - (2\mu + H)\gamma_{n+1} \end{aligned} \quad (4.25)$$

Current yield function can be written as

$$\phi_{n+1} = \|\underline{\xi}_{n+1}\| - \sqrt{\frac{2}{3}}(y_0 + \beta_{n+1}) \quad (4.26)$$

Substituting (4.25) and (4.22) into (4.26)

$$\begin{aligned} \phi_{n+1} &= \|\underline{\xi}_{n+1}^{trial}\| - (2\mu + H)\gamma_{n+1} - \sqrt{\frac{2}{3}}(y_0 + \beta_{n+1}^{trial} + h\gamma_{n+1}\sqrt{\frac{2}{3}}) \\ \phi_{n+1} &= \underbrace{\|\underline{\xi}_{n+1}^{trial}\| - \sqrt{\frac{2}{3}}(y_0 + \beta_{n+1}^{trial})}_{\phi_{n+1}^{trial}} - (2\mu + H + \frac{2}{3}h)\underbrace{\gamma_{n+1}}_{unknown} \end{aligned} \quad (4.27)$$

ϕ_{n+1}^{trial} acts as an identifier for the plastic loading. If $\phi_{n+1}^{trial} \leq 0$, the material is in the elastic domain, thus a corrector step is not necessary and $\gamma_{n+1} = 0$ since there is no plastic flow. Otherwise ($\phi_{n+1}^{trial} > 0$), the elastic domain is overstepped and a corrector step is needed to stabilize the material.

In other words, for an elastic step

$$\left. \begin{aligned} \underline{\sigma}'_{n+1} &= \underline{\sigma}'_{n+1}^{trial} \\ \underline{\beta}_{n+1} &= \underline{\beta}_{n+1}^{trial} \\ \beta_{n+1} &= \beta_{n+1}^{trial} \end{aligned} \right\} \phi_{n+1}^{trial} \leq 0 \quad (4.28)$$

For an elastoplastic step γ_{n+1} has to be computed from the consistency condition

$$\begin{aligned} \phi_{n+1} &= \phi_{n+1}^{trial} - (2\mu + H + \frac{2}{3}h)\gamma_{n+1} = 0 \\ \gamma_{n+1} &= \frac{\phi_{n+1}^{trial}}{2\mu + H + \frac{2}{3}h} \end{aligned} \quad (4.29)$$

For the plastic loading case, by inserting (4.29) into (4.22), the corrector step can be expressed as

$$\left. \begin{aligned} \sigma'_{n+1} &= \sigma_{n+1}^{trial} - \frac{2\mu\phi_{n+1}^{trial}}{2\mu + H + \frac{2}{3}h} n_{n+1} \\ \beta_{n+1} &= \beta_{n+1}^{trial} + \frac{H\phi_{n+1}^{trial}}{2\mu + H + \frac{2}{3}h} n_{n+1} \\ \beta_{n+1} &= \beta_{n+1}^{trial} + \frac{h\phi_{n+1}^{trial}}{2\mu + H + \frac{2}{3}h} \sqrt{\frac{2}{3}} \end{aligned} \right\} \text{if } \phi_{n+1}^{trial} > 0 \quad (4.30)$$

Radial return mapping algorithm with isotropic and kinematic hardening is visualized in Figure 12

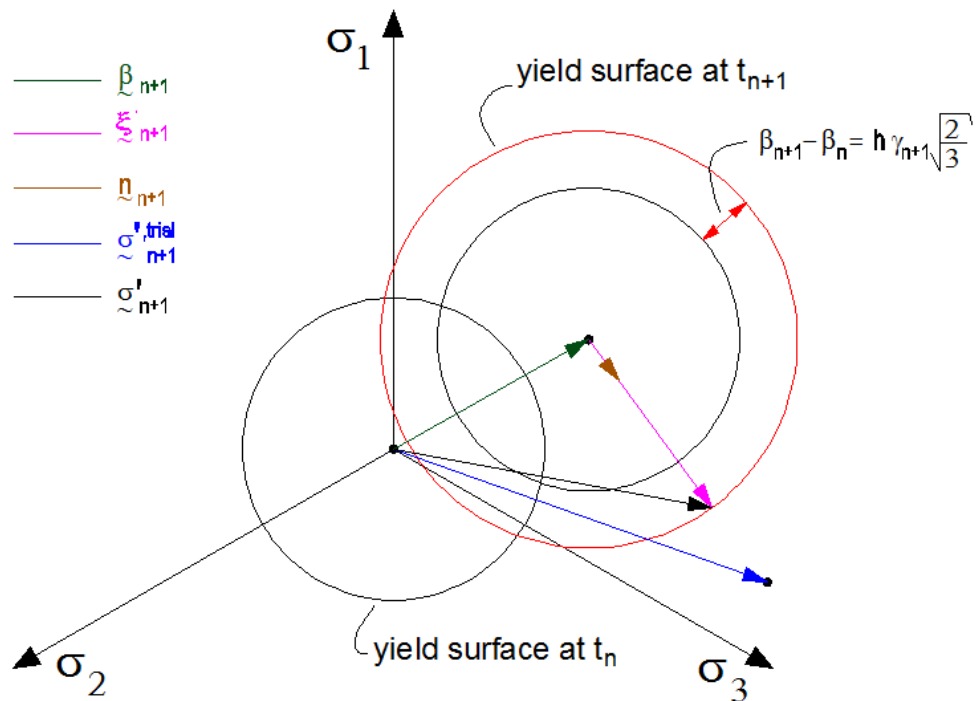


Figure 12 Visualization of the von Mises plasticity with isotropic and kinematic hardening through the principal stress state

CHAPTER 5

VERIFICATION OF THE PROPOSED BEAM ELEMENT

In this chapter, inelastic behavior and vibration characteristics of the proposed force beam element will be investigated.

There are studies concerning the inelastic behavior of FGM in literature. Bocciarelli et al. (2008) suggests the use of the J2 plasticity for metallic materials and Drucker – Prager yield condition for ceramic part; but in this work J2 plasticity will be used for both materials. In addition; the force-based finite beam element and displacement-based finite beam element formulations will be compared for different numbers of layers, integration points and elements for the study case.

The modal analysis for the FGM beam element will be compared with the ANSYS results for different length / span ratios.

5.1. COMPARISON OF INELASTIC BEHAVIORS

As mentioned above, J2 plasticity rule has been utilized for both materials for the inelastic analysis of FGM beam elements. The main difference between J2 plasticity and Drucker – Prager yield condition is; for J2 plasticity, the yield surface does not depend on the volumetric part of the stress tensor, unlike Drucker – Prager yield condition. For the one dimensional analysis case, (where the axial stress components along y and z axes and shear components along the x-z and y-z surfaces are imposed to be zero) the mentioned difference above simplifies into; the lack of the Von Mises plasticity to exhibit different yield behavior for tension and compression separately

by means of quantity, unlike the Drucker – Prager yield condition. To eliminate any mistake due to the use of J2 plasticity for ceramic part, the alumina is heavily placed in the compression zone of the beam, i.e. the top material of the beam in our example, and exposed to decrease rapidly through the depth, obeying the power law with an exponential coefficient of $n=8$. In other words, the alumina material is placed at the compression zone and it swiftly gives place to metallic material as the section move towards the bottom. The reason behind such distribution type is to minimize the misleading tensile regime of alumina material in the system; because in the tensile zone alumina will be assumed to yield at the same stress value as in the compression region, and this yield value will be far beyond its actual tensile yield strength. A substantial property of Drucker–Prager yield model is that, a change in the volumetric stress causes expansion or contraction of the yield surface. The absence of such behavior for the alumina material (since it is modeled using von Mises yield criteria in this work) will remain as a deficiency.

Primarily, the structural system for the inelastic analysis study case is visualized in Figure 13 to enlighten the further explanations about this comparative study.

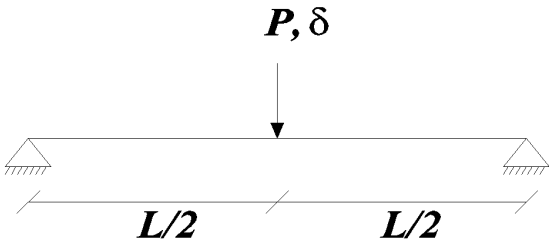


Figure 13 Inelastic Loading Example

For the inelastic case, the simply supported system shown in Figure 13 will be exposed to a displacement in the transverse $-y$ direction at the mid-span. The support conditions are pinned at both ends. The length, depth and width of the beam are 2 m, 100 mm and 100 mm, respectively. The bottom material (steel) properties are $E = 210$ GPa, $G = 80$ GPa, $\sigma_y = 500$ MPa and top material (alumina) properties are $E = 390$ GPa, $G = 137$ GPa, $\sigma_{y,compression} = 2000$ MPa and $\sigma_{y,tension} = 250$ MPa, but since von

Mises plasticity is used for alumina, yield strength is taken as the compressive strength, i.e. $\sigma_y = 2000\text{MPa}$ for both tension and compression. This assumption is also validated with the contribution of alumina to total response in terms of state of stress distributions as presented at the end of this section. The isotropic hardening parameter and kinematic hardening parameters for both materials are taken as $E \times 10^{-6}$ of each material and zero, respectively. As a result, elastic perfectly plastic material behavior is considered in the verification study.

Firstly, load vs. deflection curves for the force-based beam elements and displacement-based beam elements will be plotted (Figure 14 to Figure 19) for 3, 5, 10 Lobatto integration points (monitoring sections) through the length and 11, 21, 41 trapezoid integration points (number of layers) through the depth of section. One beam element per half-span will be used for both the force-based and the displacement-based analyses.

Another analysis for 5 Lobatto points and 41 layers with 4 force-based elements per half-span will be held out. The outcomes of this analysis are observed to be the converged nonlinear response, and are used for comparison purposes. Results are represented in Table 2.

Secondly the force-based and displacement-based beam formulations will be compared for different numbers of elements. For this analysis, the number of layers on each section and integration points along the length of each element will be determined in such a way that they minimize the error for the corresponding beam formulation type (force-based or displacement-based).

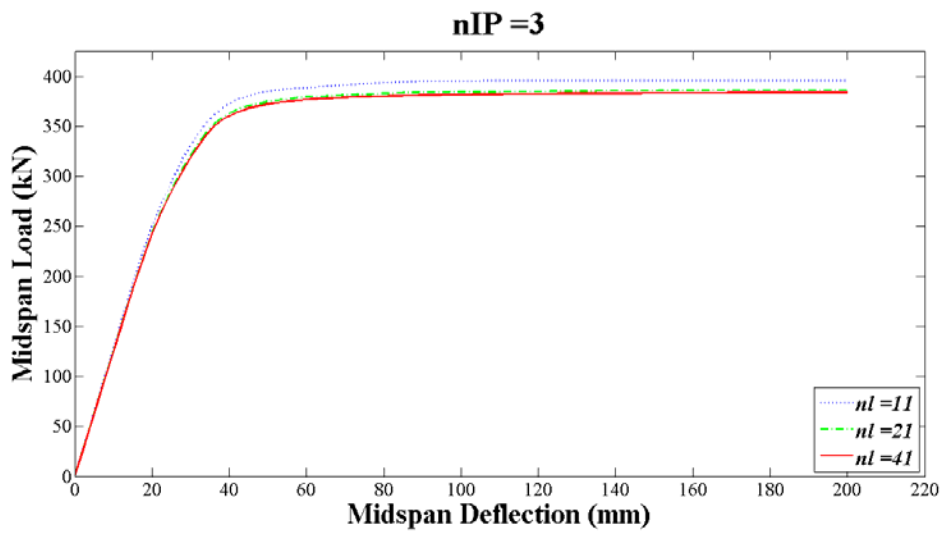


Figure 14 One force-based element per half-span and nIP = 3

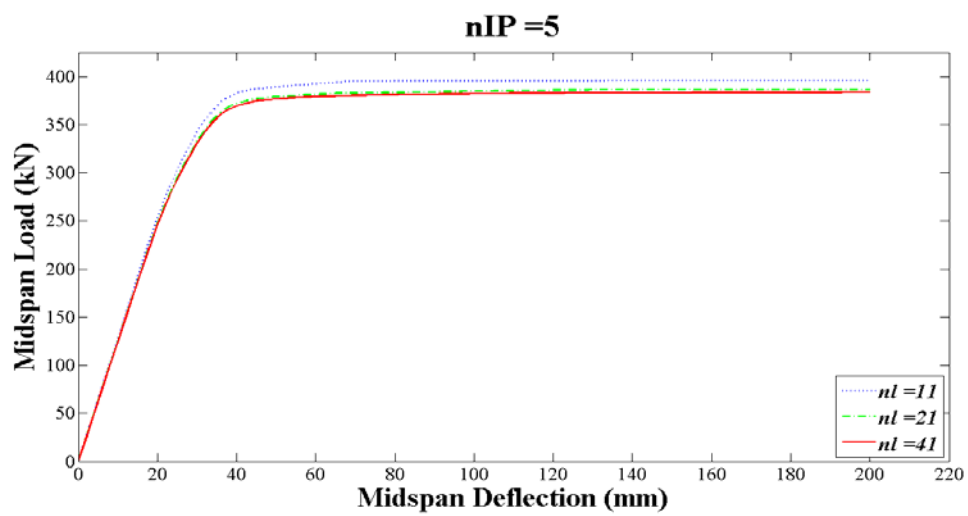


Figure 15 One force-based element per half-span and nIP = 5

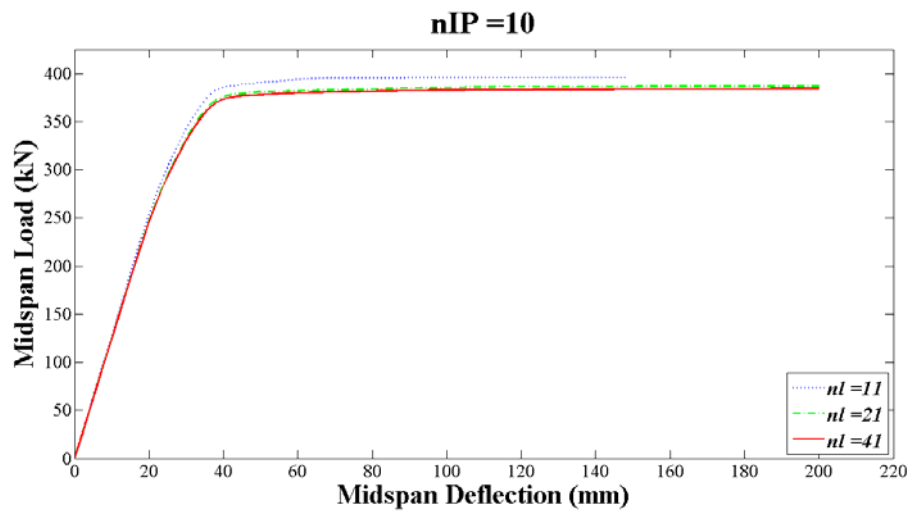


Figure 16 One force-based element per half-span and nIP = 10

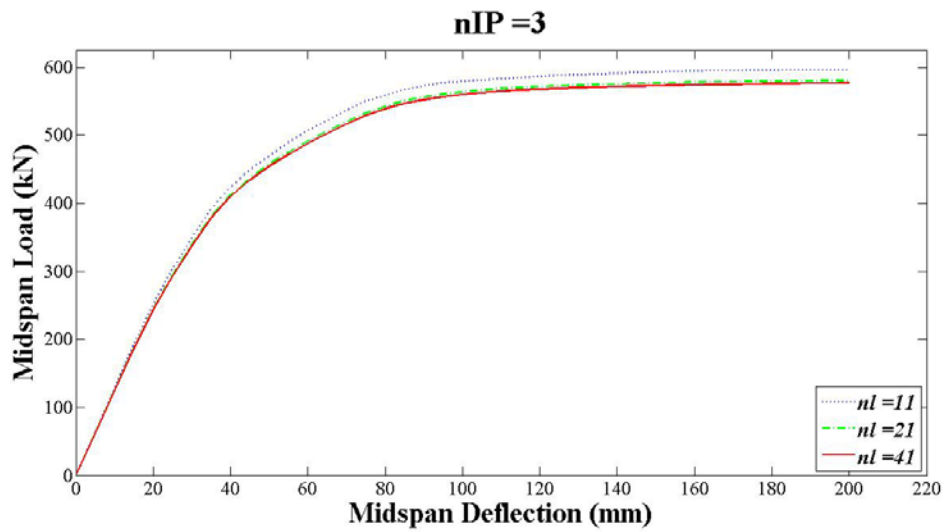


Figure 17 One displacement-based element per half-span and nIP = 3

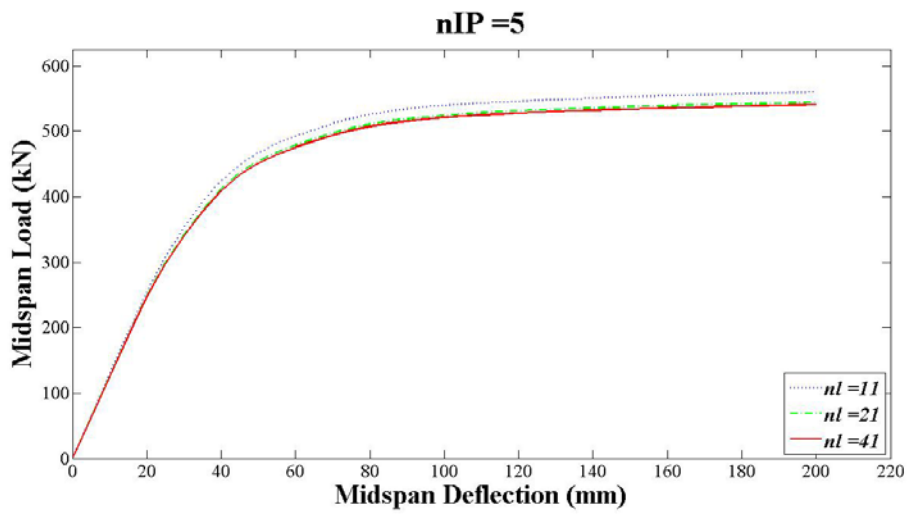


Figure 18 One displacement-based element per half-span and $nIP = 5$

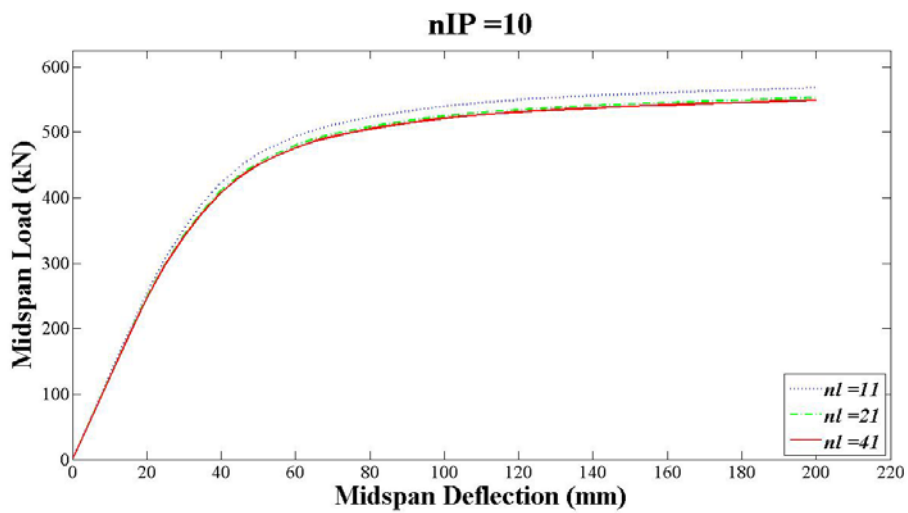


Figure 19 One displacement-based element per half-span and $nIP = 10$

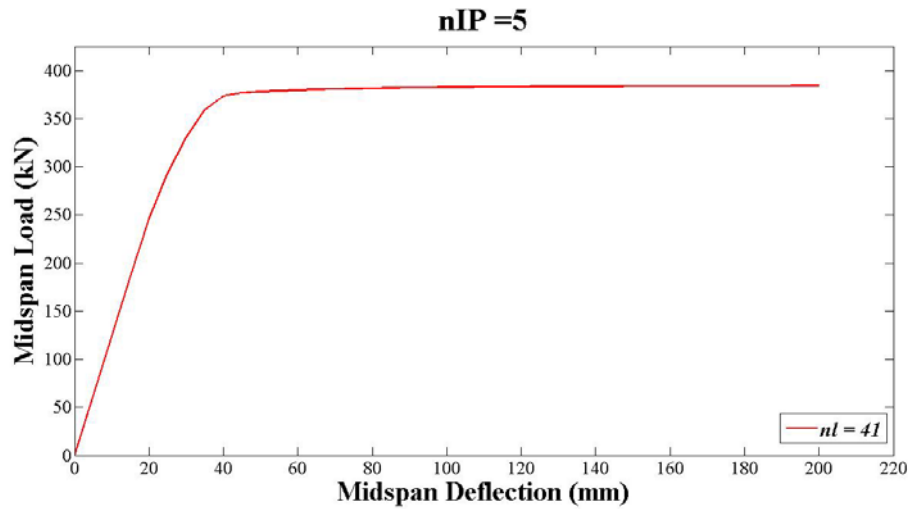


Figure 20 Four force-based elements per half-span and nIP = 5

Table 2 L/d = 5 Comparison of element responses for varying discretizations

Number of Sections (Lobatto)	Number of Layers (Trapezoidal)	Peak Mid-span Force (kN)		Error of Peak Mid-span Force		Initial Tangent Modulus (kN/mm)		Error of Initial Tangent	
		FB	DB	FB	DB	FB	DB	FB	DB
nIP = 3	nl = 11	395.663	596.620	3.03%	55.35%	12.8477	12.8477	3.48%	3.48%
	nl = 21	386.272	580.629	0.58%	51.19%	12.5027	12.5027	0.70%	0.70%
	nl = 41	383.421	576.904	0.16%	50.22%	12.4156	12.4156	0.00%	0.00%
nIP = 5	nl = 11	395.733	559.594	3.04%	45.71%	12.8477	12.8477	3.48%	3.48%
	nl = 21	386.390	544.560	0.61%	41.80%	12.5027	12.5027	0.70%	0.70%
	nl = 41	383.683	540.893	0.09%	40.84%	12.4156	12.4156	0.00%	0.00%
nIP = 10	nl = 11	395.772	567.841	3.05%	47.86%	12.8477	12.8477	3.48%	3.48%
	nl = 21	386.502	552.701	0.64%	43.92%	12.5027	12.5027	0.70%	0.70%
	nl = 41	384.064	548.810	0.01%	42.90%	12.4156	12.4156	0.00%	0.00%
	Exact Force:	384.045	4 force-based elements per half-span, 5 sections (nIP) on each element, 41						
	Exact Tangent:	12.41562	layers (nl) on each section						

As can be seen from the Table 2, increasing the number of layers decreases the error of peak mid-span force and initial tangent modulus for both force-based elements and displacement-based elements.

The number of integration points (number of sections) do not affect the initial tangent modulus. 3 Lobatto points give exact result for the integration of a 3rd degree polynomial, since n Lobatto points give exact result for the definite integration of

any polynomial with an order of $2n-3$. Integral terms that have been utilized to calculate the stiffness matrices over the length of the beam, consists at most 2^{nd} degree polynomials for both beam formulations; thus 3 Lobatto points are sufficient to calculate the exact stiffness matrices for the elastic case. Also, it can be assured from Table 2 that both beam formulations (force-based and displacement-based) ends up with the same stiffness matrices for prismatic beams with FGM inside the linear elastic domain.

For the further nonlinear analyses the number layers and sections will be kept constant and the same loading will be applied to the example problem under varying element numbers. The number of layers and number of sections will be selected as 21 and 5, respectively. The estimated errors for the force-based elements remain under 1% for the selected numbers as can be seen in Table 2. The selection also gives the second least error for displacement-based element.

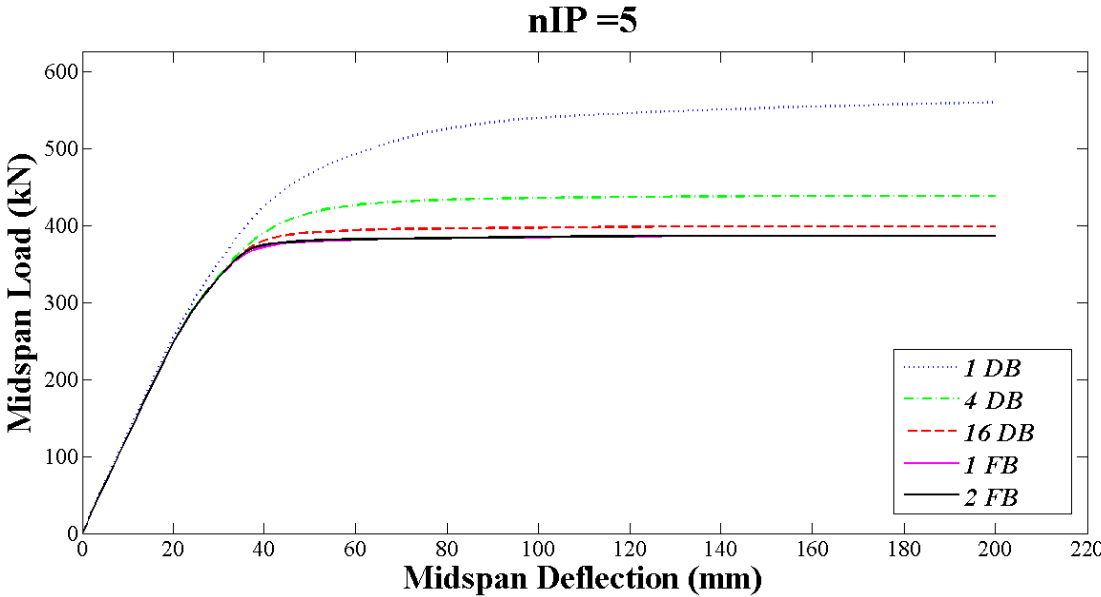


Figure 21 Load-Deflection curve for several numbers of elements (DB and FB)

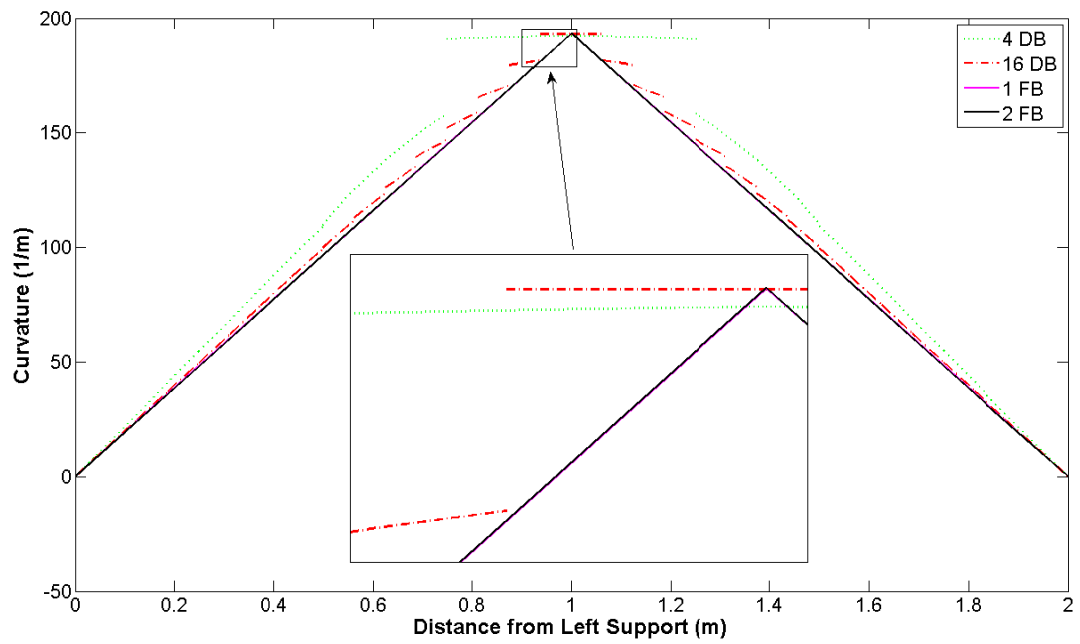


Figure 22 Bending moment distribution along the length of beam

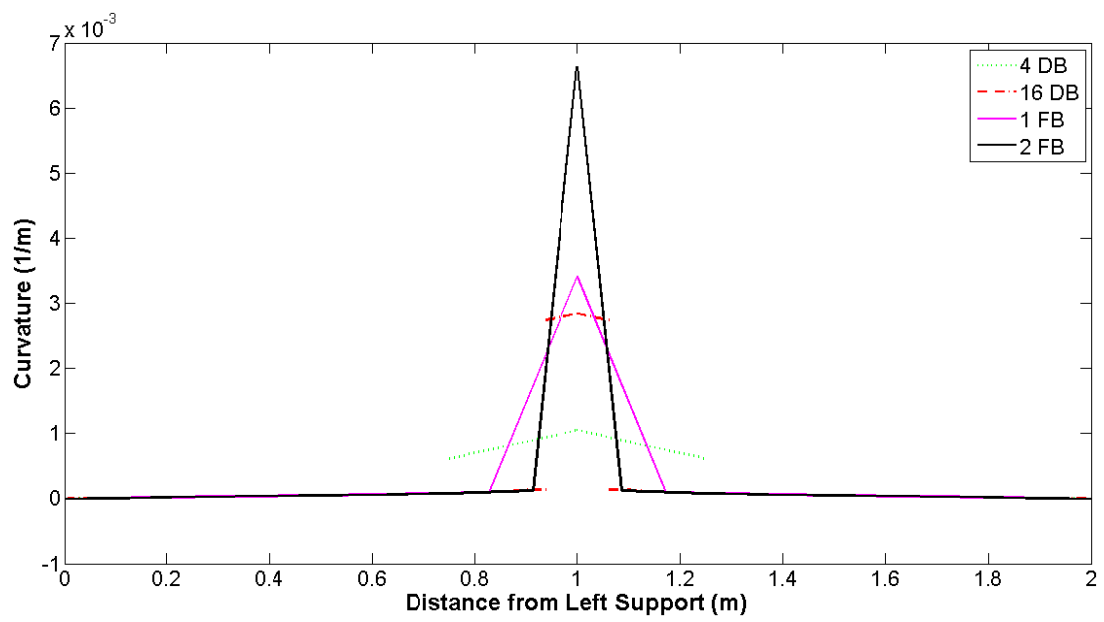


Figure 23 Curvature distribution along the length of beam

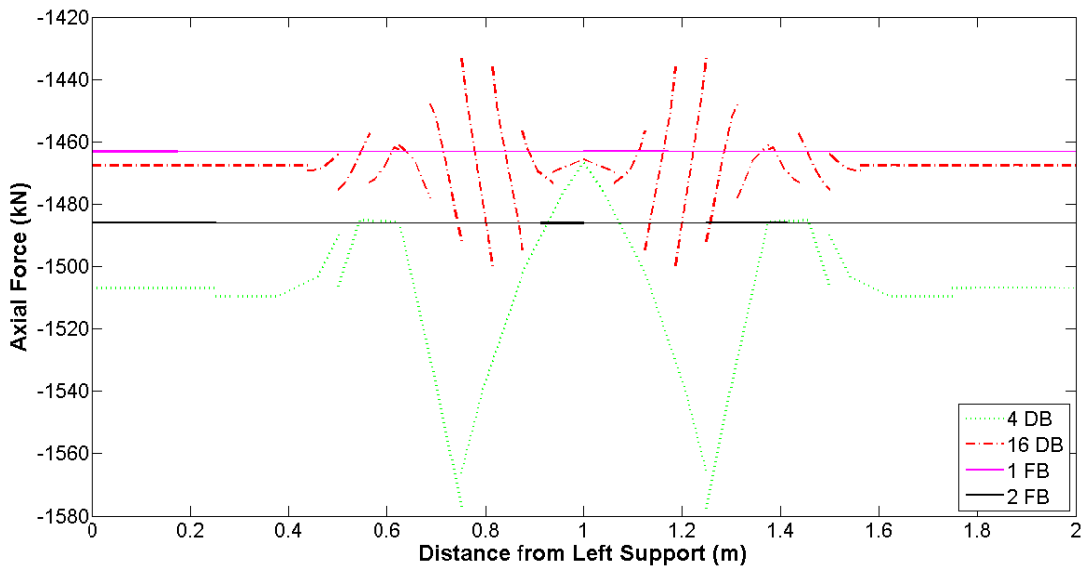


Figure 24 Axial force distribution along the length of beam

Table 3 Computation times of several analyses with different element numbers and formulation types (nIP = 5, number of layers = 21)

Number of elements per half-span	Formulation Type	Computation time (sec)
1	Displacement-based	181.75
4	Displacement-based	847.08
16	Displacement-based	4032.3
1	Force-based	268.48
2	Force-based	535.10

As presented in Figure 21, the number of elements does not affect the results significantly for force-based beam elements. The curves for 1 and 2 force-based elements per half-span are almost overlapped. On the other hand, increasing number of elements decreases the error for displacement-based formulation.

The force-based formulation gives more accurate results than displacement-based formulation. Even the solution with 16 displacement-based elements per half-span is not capable of mocking the behavior of 1 force-based element per half-span.

Speaking of the bending moment plot represented in Figure 22, as the number of displacement-based elements increases the results approach to force-based element formulation. But the displacement-based formulation does not provide a continuous solution for moment diagram unlike force-based formulation.

For the curvature diagram attached Figure 23, the discussions about error mentioned can be reclaimed; but the significant curvature difference between 1 FB and 2 FB is originated from the difference between total numbers of sections.

Considering the computation times in Table 3 and the accuracy of several analyses discussed above, one can state that using 1 force-based beam element per half-span is the most suitable option for nonlinear FEM analysis.

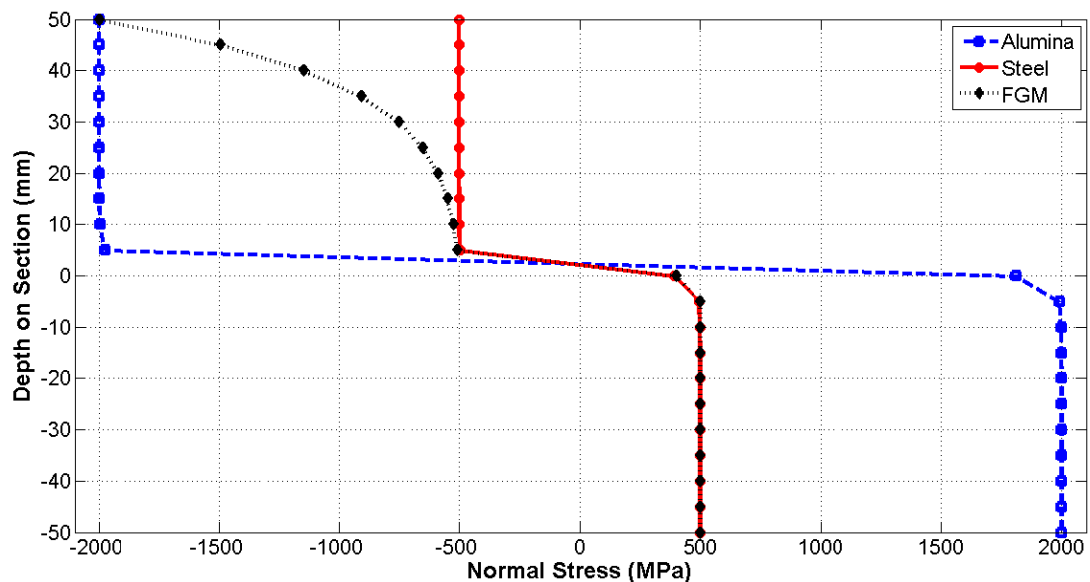


Figure 25 Normal stress distribution

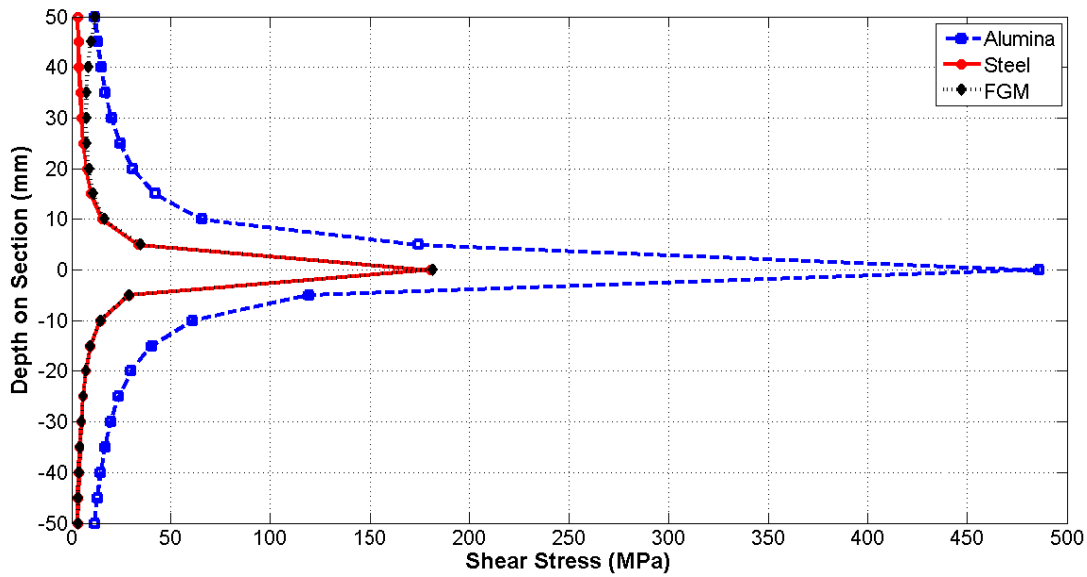


Figure 26 Shear stress distribution

The normal stress distribution and shear stress distribution through the depth of the beam with FGM are presented in Figure 25 and Figure 26, respectively. It can be indicated clearly from Figure 25 that steel material dominates the section, since a very high power coefficient has been used for the distribution ($n = 8$). Also, it can be verified that the alumina material does not contribute the section in the tensile regime, as stated in the beginning of the topic.

From Figure 25 and Figure 26, through depth of the section, shear stress tends to increase as normal stress decreases. For 2D analysis such equation ($\sigma_{11}^2 + 3\sigma_{12}^2 = \sigma_y^2$) can be obtained on the yield surface from (4.3). This equation explains the reverse relation between normal stress and shear stress.

5.2. COMPARISON OF VIBRATION CHARACTERISTICS

In this section, modal analyses will be realized for a prismatic cantilever beam. Since the cross section does not change through the length of the beam and the materials

are assumed to stay in the elastic regime; the displacement-based and force-based FGM beam formulation gives the same stiffness and mass matrices. Thus the analyses will not be held separately for each formulation types. The analyses results will be compared with a well-known FEM software package ANSYS.

The beam will be modeled using brick elements with 8 nodes via ANSYS. The mesh size will be taken as 5 mm for each brick element. Since the analyses are realized in a 3D media in ANSYS, some of the modes will be sorted out (For instance, bending and shear modes about z axis, torsion modes and modes for which warping is dominant etc). The axial modes and bending modes about y axis of the ANSYS model will be compared by means of natural frequencies and mode shapes with the proposed beam element.

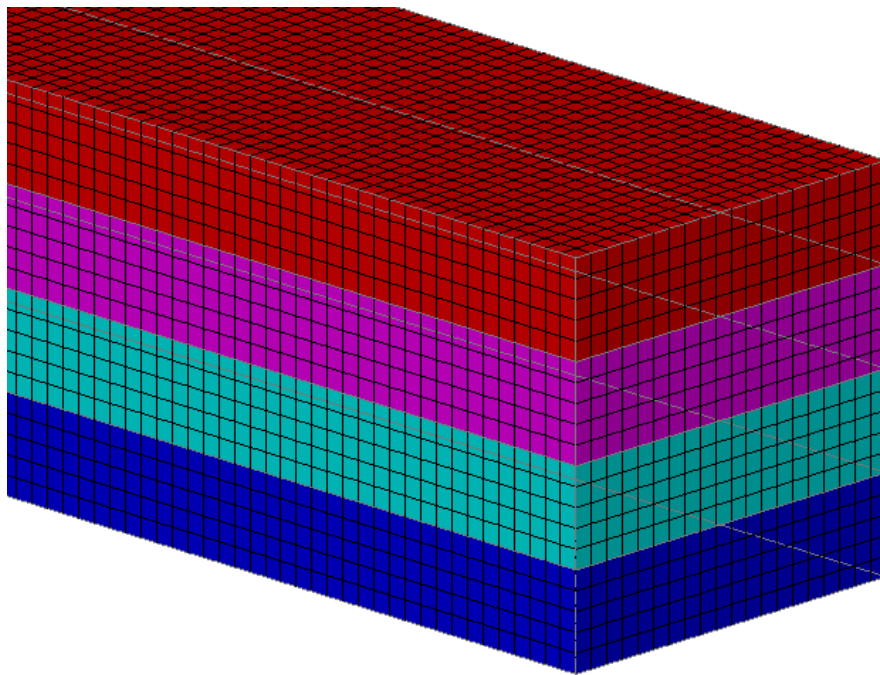


Figure 27 Visualization of ANSYS FGM beam model

The first analysis will be held out over a homogenous prismatic section made of steel. The depth and width of the section will be taken as 100 mm and 100 mm, respectively. Several analyses will be performed using different length / depth (L/d)

ratios. The steel material properties will be selected as $E = 210 \text{ GPa}$, $G = 80 \text{ GPa}$, $\rho = 7850 \text{ kg/m}^3$.

Table 4 Material properties at each layer of the ANSYS model

Section Properties (From top to bottom)	Modulus of Elasticity (GPa)	Bulk Modulus (GPa)	Mass Density (kg/m^3)
1	360.95988	128.090448	4304.0882
2	309.20578	111.971913	5110.3342
3	264.87214	97.881688	6067.6070
4	226.89501	85.564537	7204.1971

In the second analysis a beam with functionally graded material will be imitated. The beam cross section will be divided into 4 parts. The material properties for each part will be determined by using exponential law for FGM. The ANSYS model is visualized in Figure 27 and the material properties at each layer are presented in Table 4.

The top material (steel) properties are $E = 210 \text{ GPa}$, $G = 80 \text{ GPa}$, $\rho = 7850 \text{ kg/m}^3$ and bottom material (alumina) properties are $E = 390 \text{ GPa}$, $G = 137 \text{ GPa}$, $\rho = 3950 \text{ kg/m}^3$.

Table 5 $L/d = 10$ Vibration frequencies and shapes for homogenous section made of steel

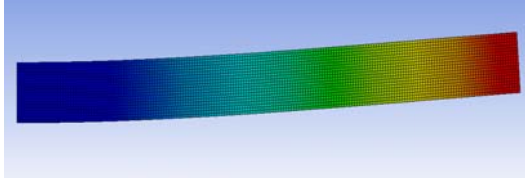
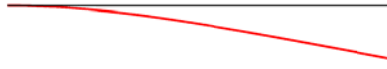
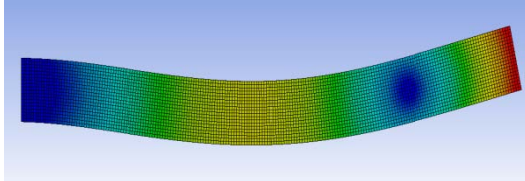
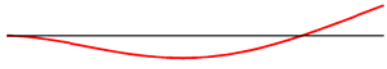
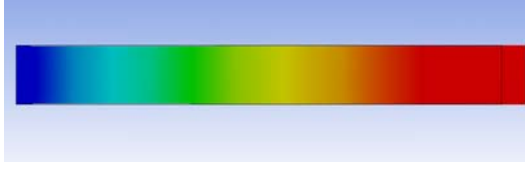

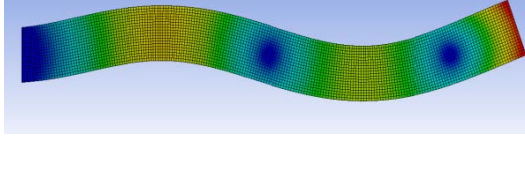
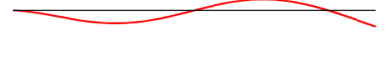
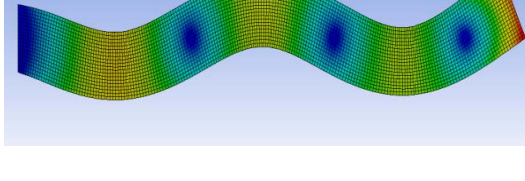

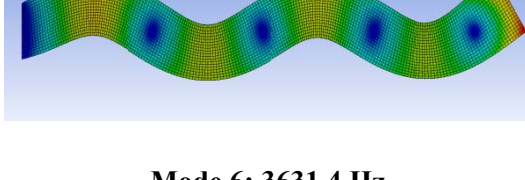

 <p>Mode 1: 83.072 Hz</p>	 <p>Mode 1: 82.885 Hz</p>
 <p>Mode 2: 498.17 Hz</p>	 <p>Mode 2: 496.634 Hz</p>
 <p>Mode 3: 1295.3 Hz</p>	 <p>Mode 3: 1293.2 Hz</p>
 <p>Mode 4: 1311.6 Hz</p>	 <p>Mode 4: 1306.1 Hz</p>
 <p>Mode 5: 2382.2 Hz</p>	 <p>Mode 5: 2369.8 Hz</p>
 <p>Mode 6: 3631.4 Hz</p>	 <p>Mode 6: 3610.9 Hz</p>

Table 5 (continued)



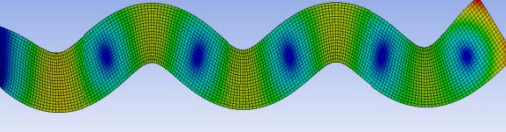
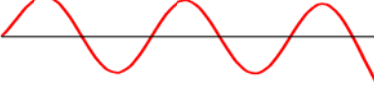
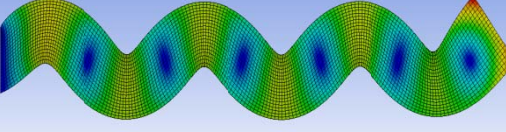
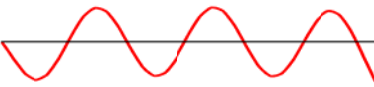
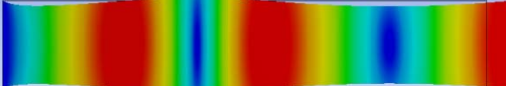

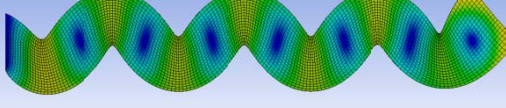

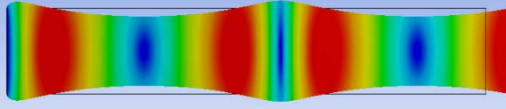

 <p>Mode 7: 3882.7 Hz</p>	 <p>Mode 7: 3882.6 Hz</p>
 <p>Mode 8: 4997.6 Hz</p>	 <p>Mode 8: 4971.0 Hz</p>
 <p>Mode 9: 6440.2 Hz</p>	 <p>Mode 9: 6413.7 Hz</p>
 <p>Mode 10: 6459.9 Hz</p>	 <p>Mode 10: 6481.5 Hz</p>
 <p>Mode 11: 7931.7 Hz</p>	 <p>Mode 11: 7916.1 Hz</p>
 <p>Mode 12: 9018.0 Hz</p>	 <p>Mode 12: 9095.9 Hz</p>

Table 6 $L/d = 5$ Vibration frequencies and shapes for homogenous section made of steel

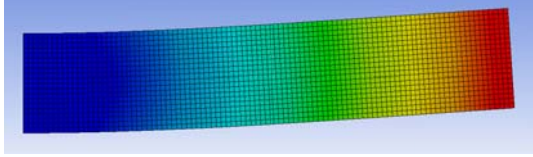
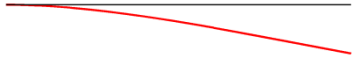
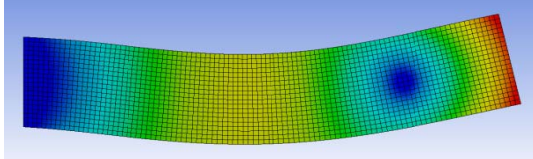
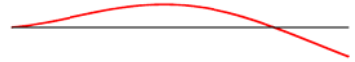
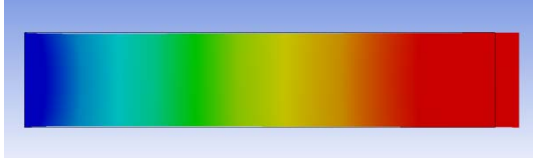

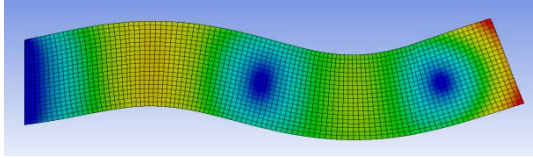

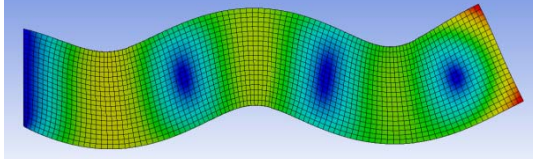
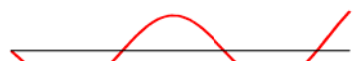
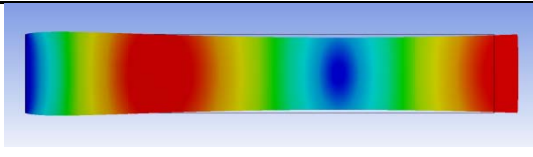

 <p>Mode 1: 325.48 Hz</p>	 <p>Mode 1: 324.02 Hz</p>
 <p>Mode 2: 1756.0 Hz</p>	 <p>Mode 2: 1743.7 Hz</p>
 <p>Mode 3: 2594.6 Hz</p>	 <p>Mode 3: 2586.3 Hz</p>
 <p>Mode 4: 4189.0 Hz</p>	 <p>Mode 4: 4150.2 Hz</p>
 <p>Mode 5: 6971.2 Hz</p>	 <p>Mode 5: 6895.6 Hz</p>
 <p>Mode 6: 7757.4 Hz</p>	 <p>Mode 6: 7765.3 Hz</p>

Table 6 (continued)

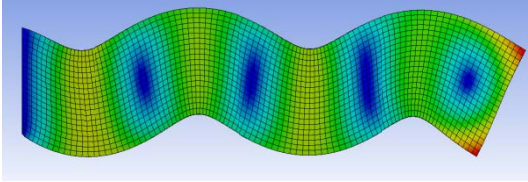
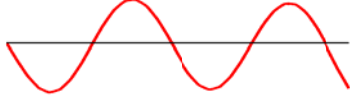
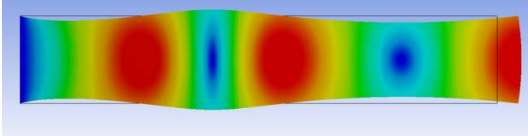

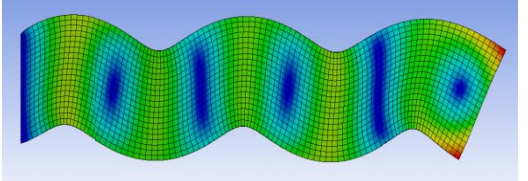
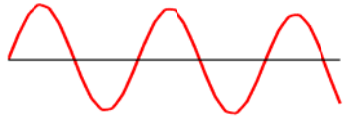
 <p>Mode 7: 9931.9 Hz</p>	 <p>Mode 7: 9822.0 Hz</p>
 <p>Mode 8: 12818.0 Hz</p>	 <p>Mode 8: 12774.9 Hz</p>
 <p>Mode 9: 12902.0 Hz</p>	 <p>Mode 9: 12962.9 Hz</p>

Table 7 $L/d = 2$ Vibration frequencies and shapes for homogenous section made of steel

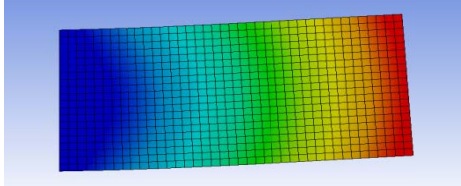
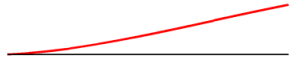
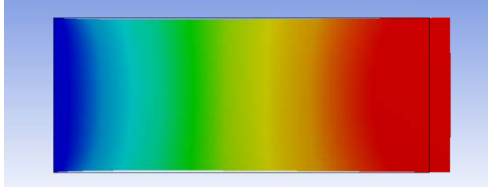

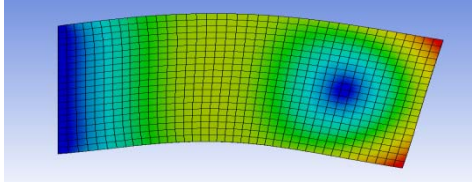
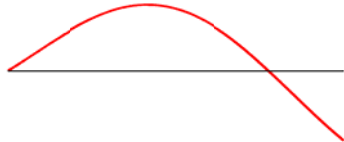
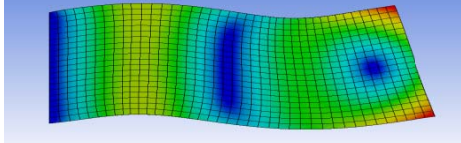

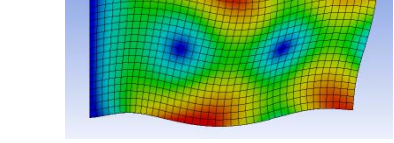
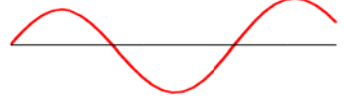
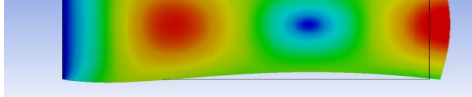

 <p>Mode 1: 1794.2Hz</p>	 <p>Mode 1: 1774.7 Hz</p>
 <p>Mode 2: 6510.4 Hz</p>	 <p>Mode 2: 6465.8 Hz</p>
 <p>Mode 3: 6813.7 Hz</p>	 <p>Mode 3: 6703.0 Hz</p>
 <p>Mode 4: 14262.0 Hz</p>	 <p>Mode 4: 14019.5 Hz</p>
 <p>Mode 5: 18232.0 Hz</p>	 <p>Mode 5: 18195.1 Hz</p>
 <p>Mode 6: 18879.0 Hz</p>	 <p>Mode 6: 19413.2Hz</p>

Table 8 L/d = 10 Vibration frequencies and shapes for 4 layers of FGM section

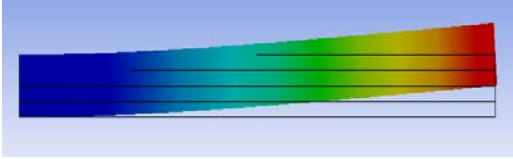
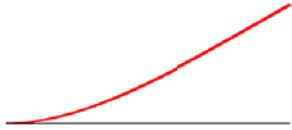
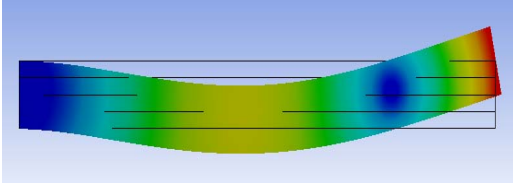
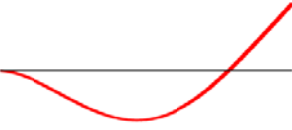
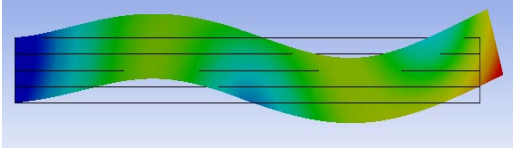
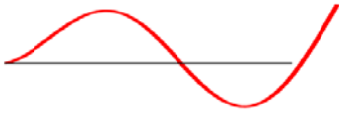
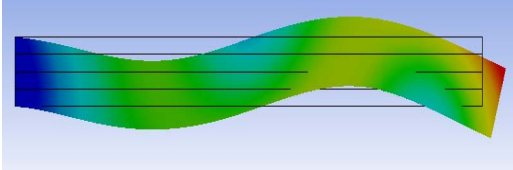
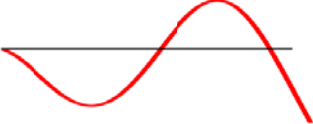
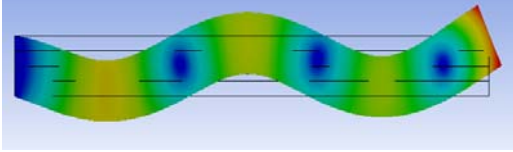
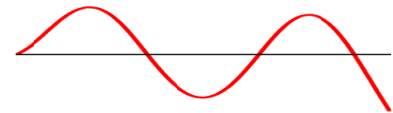
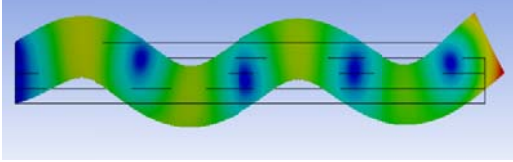
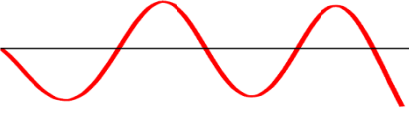
 <p>Mode 1: 113.92 Hz</p>	 <p>Mode 1: 113.67 Hz</p>
 <p>Mode 2: 681.69 Hz</p>	 <p>Mode 2: 683.56 Hz</p>
 <p>Mode 3: 1772.1 Hz</p>	 <p>Mode 3: 1778.11 Hz</p>
 <p>Mode 4: 1813.2 Hz</p>	 <p>Mode 4: 1818.63 Hz</p>
 <p>Mode 5: 3245.3 Hz</p>	 <p>Mode 5: 3295.14 Hz</p>
 <p>Mode 6: 4922.6 Hz</p>	 <p>Mode 6: 5021.85 Hz</p>

Table 8 (continued)

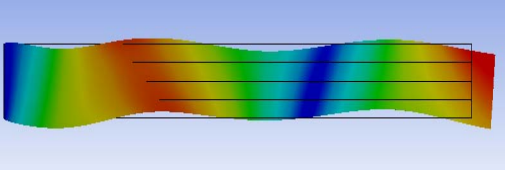
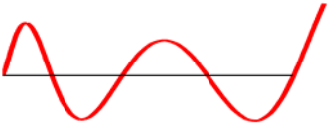
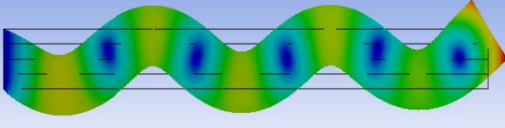
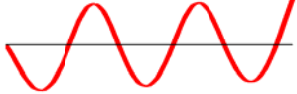
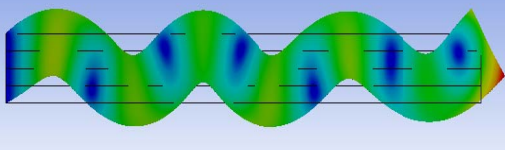
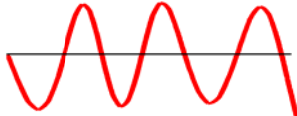
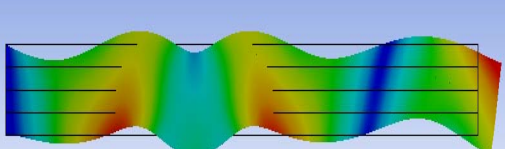
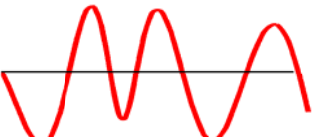
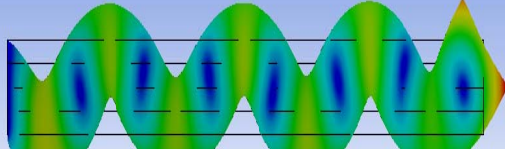
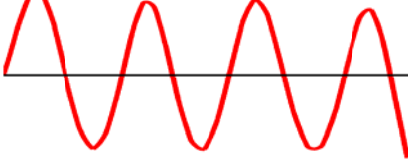
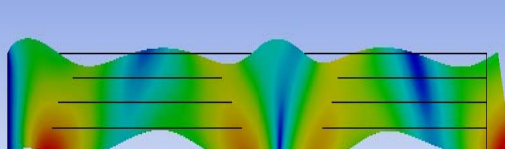
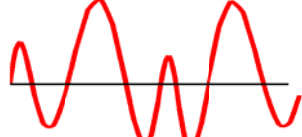
 <p>Mode 7: 5377.7 Hz</p>	 <p>Mode 7: 5390.9 Hz</p>
 <p>Mode 8: 6776.3 Hz</p>	 <p>Mode 8: 6965.39 Hz</p>
 <p>Mode 9: 8697.5 Hz</p>	 <p>Mode 9: 9043.38 Hz</p>
 <p>Mode 10: 8893.8 Hz</p>	 <p>Mode 10: 8918.44 Hz</p>
 <p>Mode 11: 10724 Hz</p>	 <p>Mode 11: 11183.3 Hz</p>
 <p>Mode 12: 12231 Hz</p>	 <p>Mode 12: 12449.4 Hz</p>

Table 9 L/d = 5 Vibration frequencies and shapes for 4 layers of FGM section

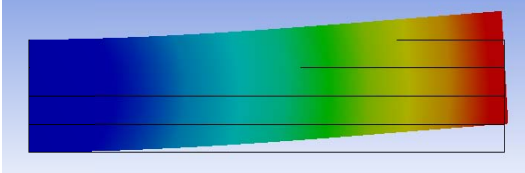
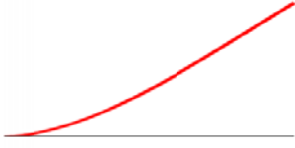
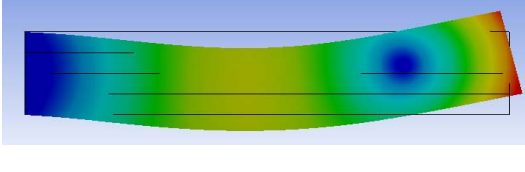


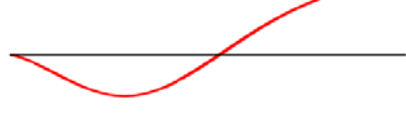
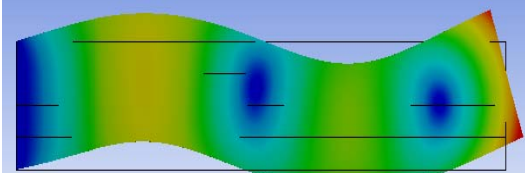
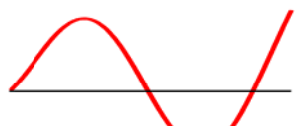
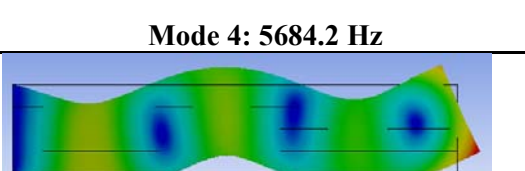

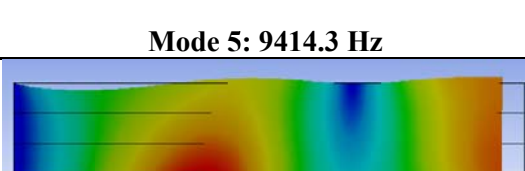

 <p>Mode 1: 446.25 Hz</p>	 <p>Mode 1: 445.25 Hz</p>
 <p>Mode 2: 2388.5 Hz</p>	 <p>Mode 2: 2417.4 Hz</p>
 <p>Mode 3: 3604.2 Hz</p>	 <p>Mode 3: 3591.6 Hz</p>
 <p>Mode 4: 5684.2 Hz</p>	 <p>Mode 4: 5812.3 Hz</p>
 <p>Mode 5: 9414.3 Hz</p>	 <p>Mode 5: 9723.5 Hz</p>
 <p>Mode 6: 10634.0 Hz</p>	 <p>Mode 6: 10688 Hz</p>

Table 9 (continued)

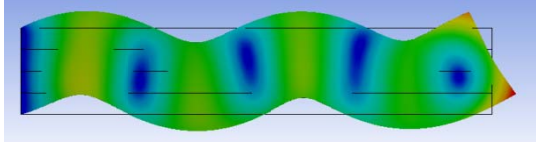
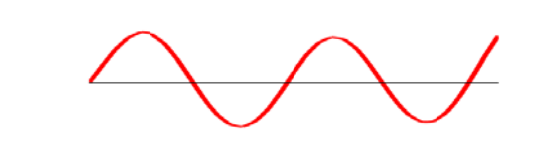
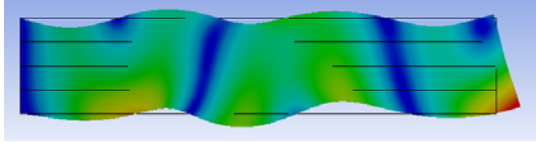
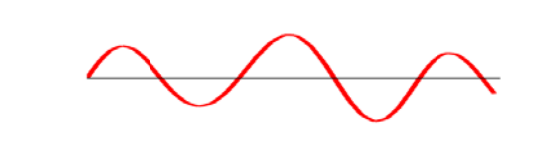
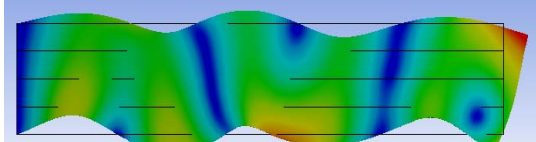
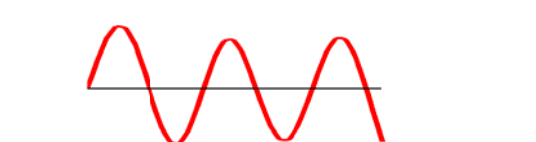
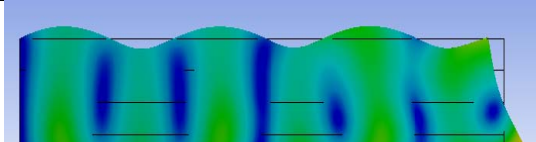
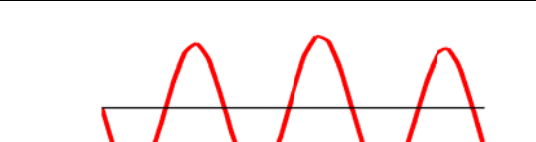
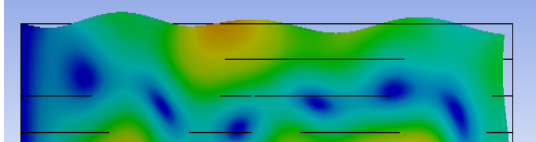
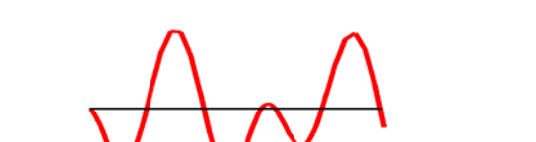
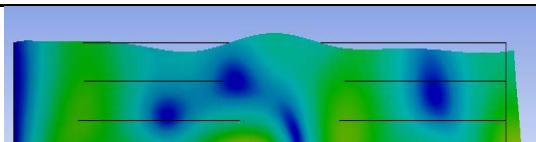
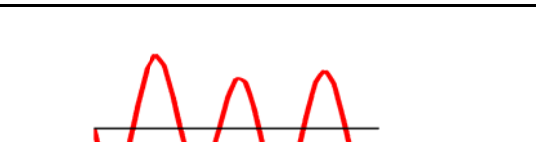
 <p>Mode 7: 13410 Hz</p>	 <p>Mode 7: 13979 Hz</p>
 <p>Mode 8: 16868 Hz</p>	 <p>Mode 8: 17364.1 Hz</p>
 <p>Mode 9: 17603 Hz</p>	 <p>Mode 9: 18542 Hz</p>
 <p>Mode 10: 20871 Hz</p>	 <p>Mode 10: 22392 Hz</p>
 <p>Mode 11: 22380 Hz</p>	 <p>Mode 11: 24320 Hz</p>
 <p>Mode 12: 23074 Hz</p>	 <p>Mode 12: 25340 Hz</p>

Table 10 L/d = 2 Vibration frequencies and shapes for 4 layers of FGM section

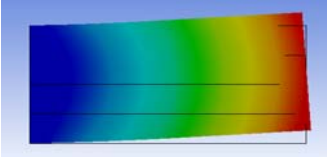
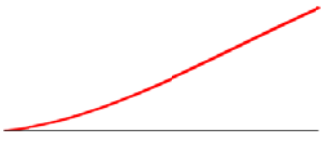
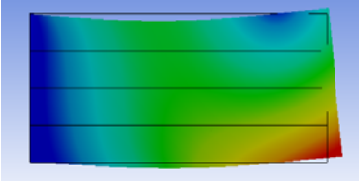
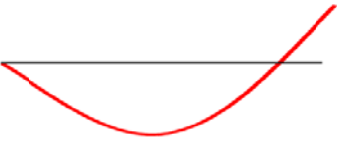
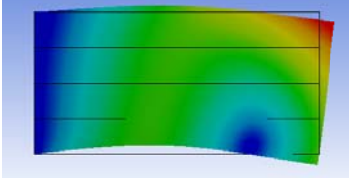
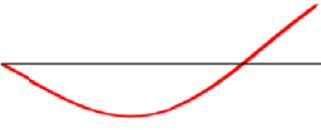
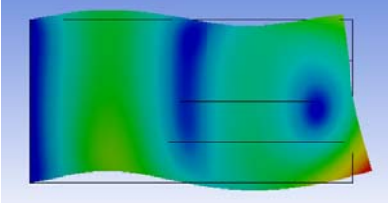
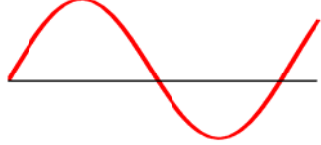
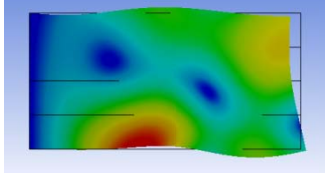
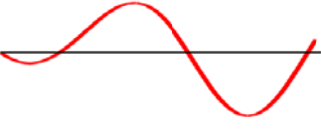
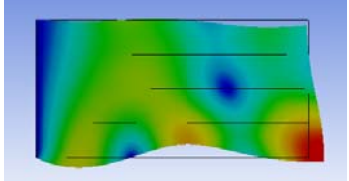
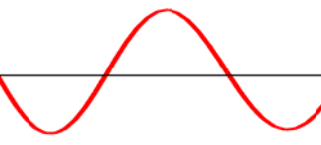
 <p>Mode 1: 2450.1 Hz</p>	 <p>Mode 1: 2463.04 Hz</p>
 <p>Mode 2: 8527.3 Hz</p>	 <p>Mode 2: 8523.3 Hz</p>
 <p>Mode 3: 9753.4 Hz</p>	 <p>Mode 3: 10036.0 Hz</p>
 <p>Mode 4: 18969 Hz</p>	 <p>Mode 4: 19785.8 Hz</p>
 <p>Mode 5: 23908 Hz</p>	 <p>Mode 5: 25676 Hz</p>
 <p>Mode 6: 25022 Hz</p>	 <p>Mode 6: 27398 Hz</p>

Table 11 Frequency comparison of proposed beam element and ANSYS model for rectangular steel section d=100 mm and b=100 mm

L/d	Mode	Steel Section				
		Beam Element SCF=5/6	Beam Element SCF=1	ANSYS Model Natural	Error SCF=5/6	Error SCF=1
10	1	82.89	82.97	83.072	0.23%	0.13%
	2	496.6	499.8	498.17	0.31%	0.33%
	3	1293.2	1293.2	1295.3	0.16%	0.16%
	4	1306.1	1323.3	1311.6	0.42%	0.89%
	5	2369.8	2418.8	2382.2	0.52%	1.54%
	6	3610.9	3710.4	3631.4	0.56%	2.18%
	7	3882.6	3882.7	3882.7	0.00%	0.00%
	8	4971.0	5138.1	4997.6	0.53%	2.81%
	9	6413.7	6481.5	6440.2	0.41%	0.64%
	10	6481.5	6662.9	6459.9	0.33%	3.14%
	11	7916.1	8259.4	7931.7	0.20%	4.13%
	12	9095.9	9095.9	9018	0.86%	0.86%
5	1	324.02	325.25	325.48	0.45%	0.07%
	2	1743.7	1778.7	1756	0.70%	1.30%
	3	2586.3	2586.4	2594.6	0.32%	0.32%
	4	4150.2	4286.0	4189	0.93%	2.32%
	5	6895.6	7191.2	6971.2	1.08%	3.16%
	6	7765.3	7765.3	7757.4	0.10%	0.10%
	7	9822.0	10314.3	9931.9	1.11%	3.85%
	8	12774.9	12963.0	12818	0.34%	1.13%
	9	12962.9	13503.0	12902	0.47%	4.66%
2	1	1774.7	1807.1	1794.2	1.09%	0.72%
	2	6465.8	6465.9	6510.4	0.69%	0.68%
	3	6703.0	7036.0	6813.7	1.62%	3.26%
	4	14019.5	14817.5	14262	1.70%	3.90%
	5	18195.1	19413.3	18232	0.20%	6.48%
	6	19413.2	19594.8	18879	2.83%	3.79%

Table 12 Frequency comparison of proposed beam element and ANSYS model for FGM section d=100 mm and b=100 mm

L/d	Mode	Top Alumina - Bottom Ceramics FGM Section		
		Beam Element SCF=1 Natural Frequencies (Hz)	ANSYS Model Natural Frequencies (Hz)	Error
10	1	113.67	113.92	0.22%
	2	683.56	681.69	0.27%
	3	1778.11	1772.1	0.34%
	4	1818.63	1813.2	0.30%
	5	3295.14	3245.3	1.54%
	6	5021.85	4922.6	2.02%
	7	5390.9	5377.7	0.25%
	8	6965.39	6776.3	2.79%
	9	9043.38	8697.5	3.98%
	10	8918.44	8893.8	0.28%
	11	11183.3	10724	4.28%
	12	12449.4	12231	1.79%
5	1	445.25	446.25	0.22%
	2	2417.4	2388.5	1.21%
	3	3591.6	3604.2	0.35%
	4	5812.3	5684.2	2.25%
	5	9723.5	9414.3	3.28%
	6	10688	10634	0.51%
	7	13979	13410	4.24%
	8	17364.1	16868	2.94%
	9	18542	17603	5.33%
	10	22392	20871	7.29%
	11	24320	22380	8.67%
	12	25340	23074	9.82%
2	1	2463.04	2450.1	0.53%
	2	8523.3	8527.3	0.05%
	3	10036	9753.4	2.90%
	4	19785.8	18969	4.31%
	5	25676	23908	7.40%
	6	27398	25022	9.50%

The modal analyses results for steel section are presented in Table 11.

As the length/depth ratio decreases, shear deformations turn out to be more deterministic on the results of analyses. The proposed beam element is constituted in accordance with Timoshenko's beam theory. Since the plane sections remain plane after deformation the beam is not capable of mocking the realistic shear deformations. This lack of behavior for the beam element ends up with a statement that as the length/depth ratio decreases the natural frequency error increases. On the other hand for the axial modes the beam element gives less than 1% error even for $L/d=2$.

Speaking of the FGM section, the same statements can be put forward for the error values given in Table 12. In addition, the bending - axial coupling terms, aroused in the evolution of FGM finite element formulation, end up with complicated mode shapes. Such behavior of FGM makes it difficult to match between the modes of ANSYS and the proposed beam element especially for fewer values of L/d .

CHAPTER 6

CONCLUSIONS

6.1. SUMMARY

The main purpose of this thesis is to represent a new force-based beam finite element to be used in the analysis of functionally graded materials. For this purpose, force-based formulation has been adapted to be compatible with a typical FGM section, where the material properties vary through depth of the section. The proposed force-based beam element has been compared with a previously developed displacement-based beam finite element for regarding the non-linear behavior. Also vibration analysis of the proposed beam element is verified with ANSYS results using 3D solid elements.

6.2. CONCLUSIONS

- The elastic behavior of the force-based element and the displacement beam element yields the same results.
- For the inelastic analyses of beams with FGM, 1 force-based element per half span yields an error less than 1% whereas the error of 1 displacement-based element per half span is about 40%.
- For the vibration analyses, as length/depth ratio increases the errors for frequencies of the proposed beam element tends to decrease.
- The proposed beam element is able to determine even the axial-bending mixed mode shapes and frequencies for $L/d=10$ and $L/d=5$.

- It is getting more insistent to match the complex mode shapes as length/depth ratio decreases.

6.3. RECOMMENDATIONS FOR FUTURE STUDY

For the yield behavior of alumina material in FGM model, Drucker–Prager yield criteria can be utilized. By this means the proposed beam’s mechanical behavior can be more realistic.

Thermo-mechanical analyses should be realized in order to investigate the distribution of the temperature field under specified heat and/or body loadings.

In addition, a parametric study for functionally graded materials can be held out by means of finite element analysis, to be utilized in the design process of FGM beams.

REFERENCES

- Bocciarelli, M., G. Bolzon and G. Maier (2008). "A constitutive model of metal–ceramic functionally graded material behavior: Formulation and parameter identification." Computational Materials Science **43**(1): 16-26.
- Chakraborty, A., S. Gopalakrishnan and J. N. Reddy (2003). "A new beam finite element for the analysis of functionally graded materials." International Journal of Mechanical Sciences **45**(3): 519-539.
- Filippou, F. C. and G. L. Fenves (2004). *Methods of Analysis for Earthquake-Resistant Structures. Earthquake Engineering, From Engineering Seismology to Performance-Based Engineering*. Y. Bozorgnia and V. V. Bertero, CRC Press LLC.
- Friedman, Z. and J. B. Kosmatka (1993). "An improved two-node timoshenko beam finite element." Computers & Structures **47**(3): 473-481.
- Hemmatnezhad, M., R. Ansari and G. H. Rahimi (2013). "Large-amplitude free vibrations of functionally graded beams by means of a finite element formulation." Applied Mathematical Modelling **37**(18–19): 8495-8504.
- Jha, D. K., T. Kant and R. K. Singh (2013). "A critical review of recent research on functionally graded plates." Composite Structures **96**(0): 833-849.
- Kieback, B., A. Neubrand and H. Riedel (2003). "Processing techniques for functionally graded materials." Materials Science and Engineering: A **362**(1–2): 81-106.
- Mohanty, S. C., R. R. Dash and T. Rout (2011). "Parametric instability of a functionally graded Timoshenko beam on Winkler's elastic foundation." Nuclear Engineering and Design **241**(8): 2698-2715.
- Molins, C., P. Roca and A. H. Barbat (1998). "Flexibility-based linear dynamic analysis of complex structures with curved-3D members." Earthquake Engineering & Structural Dynamics **27**(7): 731-747.

- Nakamura, T., T. Wang and S. Sampath (2000). "Determination of properties of graded materials by inverse analysis and instrumented indentation." Acta Materialia **48**(17): 4293-4306.
- Reddy, J. N. (1997). "On locking-free shear deformable beam finite elements." Computer Methods in Applied Mechanics and Engineering **149**(1-4): 113-132.
- Reddy, J. N. (2000). "Analysis of functionally graded plates." International Journal for Numerical Methods in Engineering **47**(1-3): 663-684.
- Reddy, J. N. and C. D. Chin (1998). "Thermomechanical analysis of functionally graded cylinders and plates." Journal of Thermal Stresses **21**(6): 593-626.
- Saritas, A. (2006). Mixed Formulation Frame Element for Shear Critical Steel and Reinforced Concrete Members. Ph.D. Dissertation, University of California , Berkeley.
- Saritas, A. and O. Soydas (2012). "Variational base and solution strategies for non-linear force-based beam finite elements." International Journal of Non-Linear Mechanics **47**(3): 54-64.
- Soydas, O. (2013). A three dimensional mixed formulation nonlinear frame finite element based on Hu-Washizu functional. Ph.D., METU.
- Soydas, O. and A. Saritas (2013). "An accurate nonlinear 3d Timoshenko beam element based on Hu-Washizu functional." International Journal of Mechanical Sciences **74**(0): 1-14.
- Spacone, E., V. Ciampi and F. C. Filippou (1996). "Mixed formulation of nonlinear beam finite element." Computers & Structures **58**(1): 71-83.

APPENDIX A

DEFINITION OF VARIATION

Total energy functional is indicated in (3.4) and (3.5). The formulation will be derived according to minimization of energy functional.

$$P = S + T = \frac{1}{2} \int_0^L \int_A [(\sigma_x \varepsilon_x + \tau_{xy} \gamma_{xy}) + \rho(y)(\dot{U}^2 + \dot{W}^2)] dA dx \quad (A.1)$$

The variation of a functional $F(u, w, \phi)$ with respect to u is

$$\delta u = \lim_{\varepsilon \rightarrow 0} \frac{F(u + \varepsilon v, w, \phi) - F(u, w, \phi)}{\varepsilon} \quad (A.2)$$

where v is the test function that satisfies essential boundary conditions of the corresponding differential equation.

Using (3.1),(3.2) and (3.3)

$$P(u, w, \phi) = \frac{1}{2} \int_0^L \int_A \left(E(y)(u_{,x} - y\phi_{,x})^2 + G(y)(-\phi + w_{,x})^2 + \dots \right. \\ \left. + \rho(y)((\dot{u} - y\dot{\phi})^2 + (\dot{w})^2) \right) dA dx \quad (A.3)$$

taking the derivative of (A.3) with respect to u

$$\delta u = \frac{\frac{1}{2} \int_0^L \int_A (E(y)((u + \varepsilon v)_{,x} - y\phi_{,x})^2 + G(y)(-\phi + w_{,x})^2 + \rho(y)((\dot{u} + \varepsilon \dot{v}) - y\dot{\phi})^2 + (\dot{w})^2) dA dx - P(u, w, \phi)}{\varepsilon}$$

$$\delta u = \frac{\frac{1}{2} \int_0^L \int_A [E(y)\varepsilon(2u_{,x} v_{,x} - 2y\phi_{,x} v_{,x}) + \rho(y)\varepsilon(2\dot{u}\dot{v} - 2y\dot{\phi}\dot{v})] dA dx}{\varepsilon} \quad (A.4)$$

$$\delta u = \frac{1}{2} \int_0^L \int_A [E(y)(2u_{,x} v_{,x} - 2y\phi_{,x} v_{,x}) + \rho(y)(2\dot{u}\dot{v} - 2y\dot{\phi}\dot{v})] dA dx$$

Applying integration by parts for the terms $\int_0^L u_{,x} v_{,x} dx = u_{,x} v \Big|_0^L - \int_0^L u_{,xx} v dx$ and

$\int_0^L \phi_{,x} v_{,x} dx = \phi_{,x} v \Big|_0^L - \int_0^L \phi_{,xx} v dx$, (A.4) will transform into

$$\begin{aligned} \delta u = & \int_0^L \int_A v [E(y)(-u_{,xx} + y\phi_{,xx}) + \rho(y)(-\ddot{u} + y\ddot{\phi})] dA dx \\ & + \left[\int_A v(x) [E(y)(u(x)_{,x} - y\phi(x)_{,x}) + \rho(y)(\dot{u}(x) - y\dot{\phi}(x))] dA \right]_0^L \end{aligned} \quad (A.5)$$

The terms in the last row of (A.5) are either representing the external forces or zero depending on the boundary condition type of the freedom (EBC or NBC)

If the boundary condition type is essential, the term mentioned above will be zero since the test functions have to satisfy the essential boundary conditions of the corresponding differential equation ($v(x_{EBC}) = 0$). Otherwise the term clearly represents the external forces since the shape functions are constituted in such a way that they yield $v(x_{NBC}) = 1$ at natural boundary conditions according to finite element shape functions.

After handling the mentioned term above; substituting the terms defined in (3.7) into (A.5) yields

$$\delta u : I_0 \ddot{u} - I_1 \ddot{\phi} - A_{11} u_{,xx} + B_{11} \phi_{,xx} \quad (A.6)$$

The same procedure (taking derivative of $P(u, w, \phi)$ with respect to w and ϕ) can be applied to acquire the other terms of (3.9).